Testing the Physics of Solar and Stellar Flares with NASA's Solar Dynamics Observatory and Radiative MHD Simulations

Mark Cheung, Lockheed Martin Solar & Astrophysics Lab, Palo Alto, CA, USA

Webinar of Global Reach, Feb 5th 2020

cheung@lmsal.com

Broad Science Questions

- What are the physical mechanisms that:
  - drive the build-up of magnetic energy in the solar corona to cause flares and eruptions?
  - channel the abrupt release of stored magnetic energy into other forms, which are ultimately responsible for the salient observational signatures common to flares (e.g. increase in X-ray and EUV fluxes by orders of magnitudes)?
- How, and what do we learn about the temperature structure and evolution of coronal (namely million K) plasma using EUV and X-ray observations?
- What lessons do we learn from studying the solar atmosphere that can be applied to other astrophysical systems, e.g. stellar activity?
- Heads-up: This talk does not cover particle acceleration.

Coronal mass ejection (CME) and flare in SDO/AIA

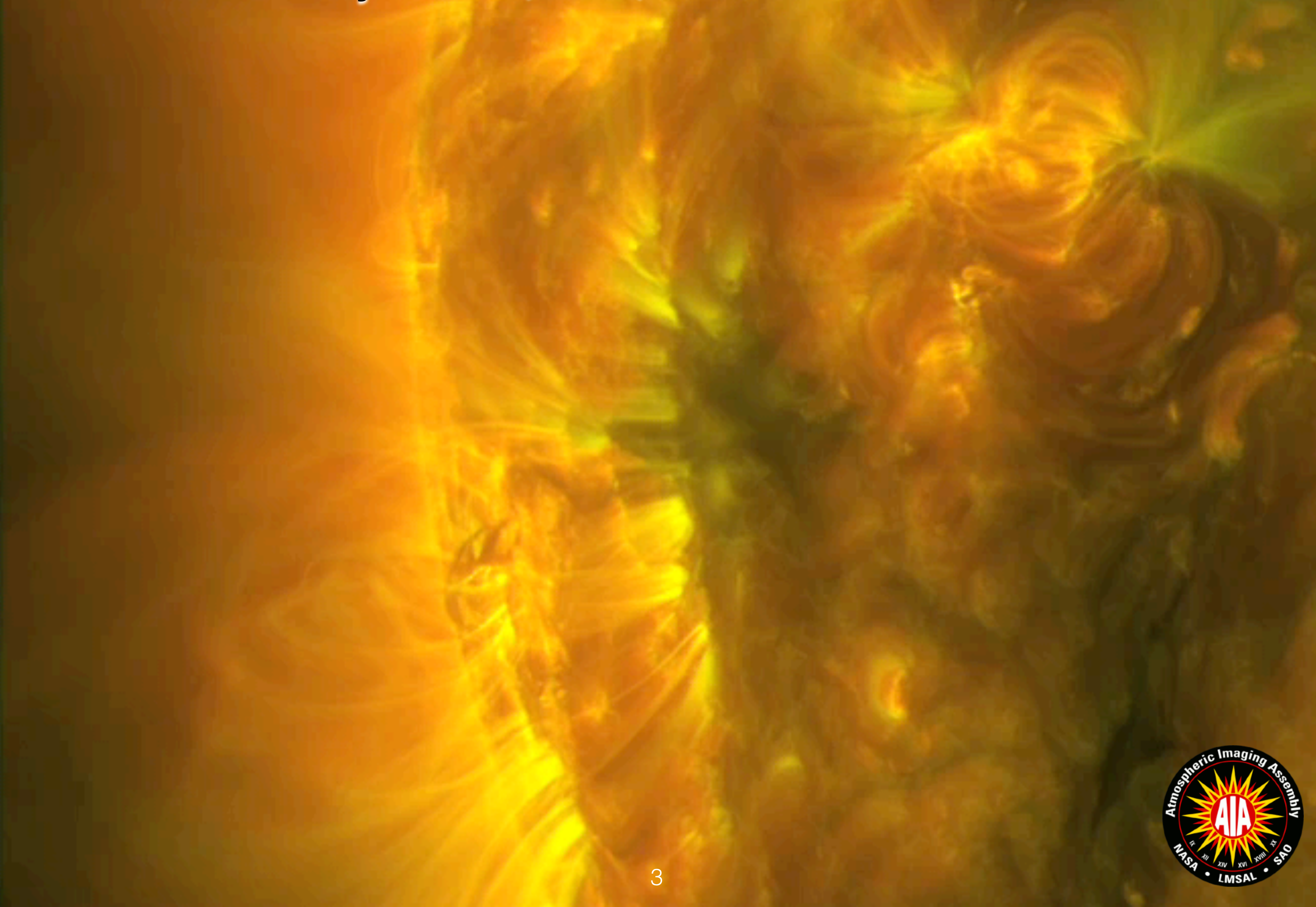

Downs et al. "Probing the solar magnetic field with a sungrazing comet", Science, 340, 1196 (2013)

NASA SDO and STEREO EUV observations of the 2011 swing-by of Comet Lovejoy, compared with magnetic coronal modeling.

See also Bryans & Pesnell (2012) and McCauley et al. (2013) for emission mechanisms from outgassed material.

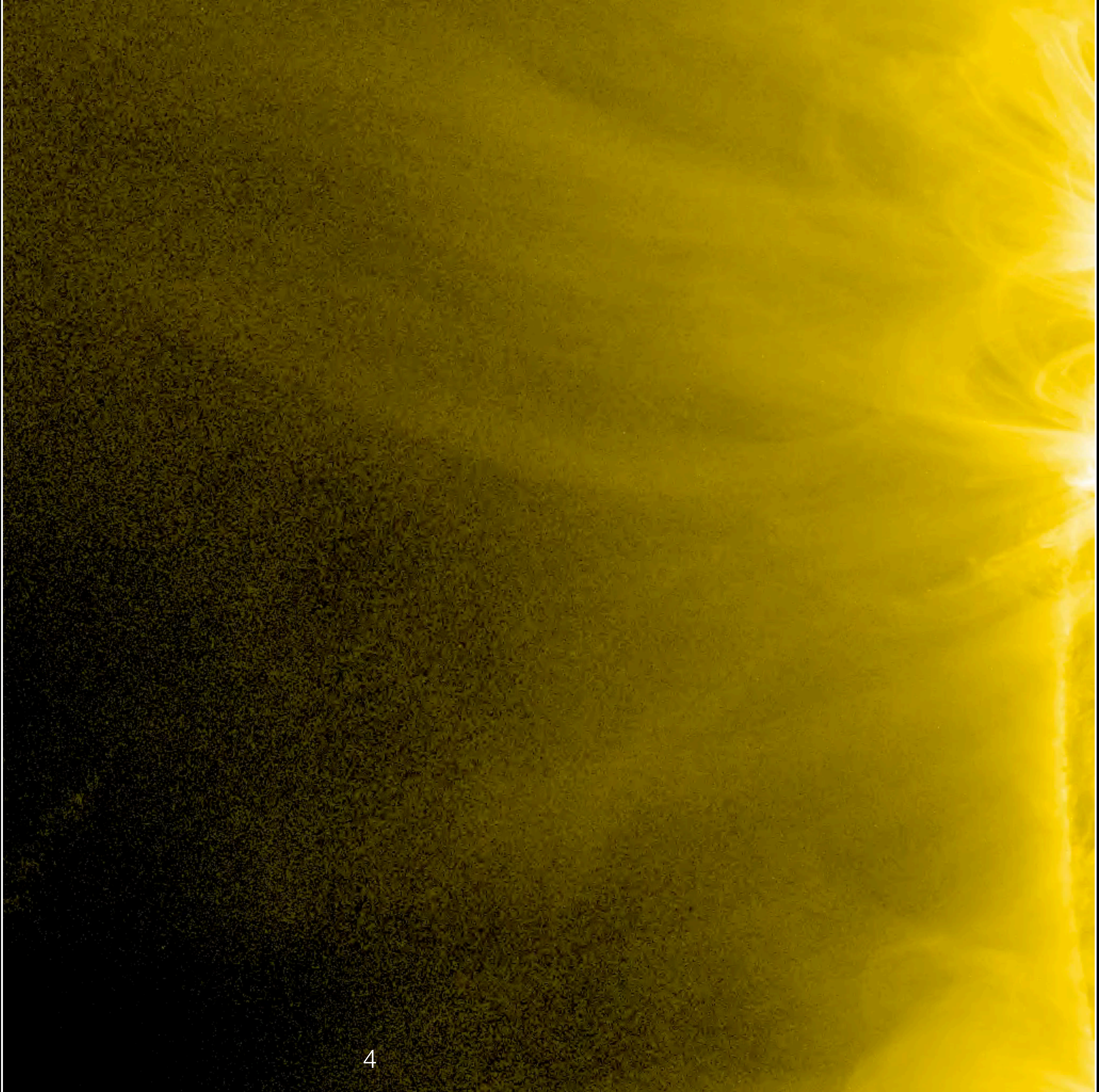

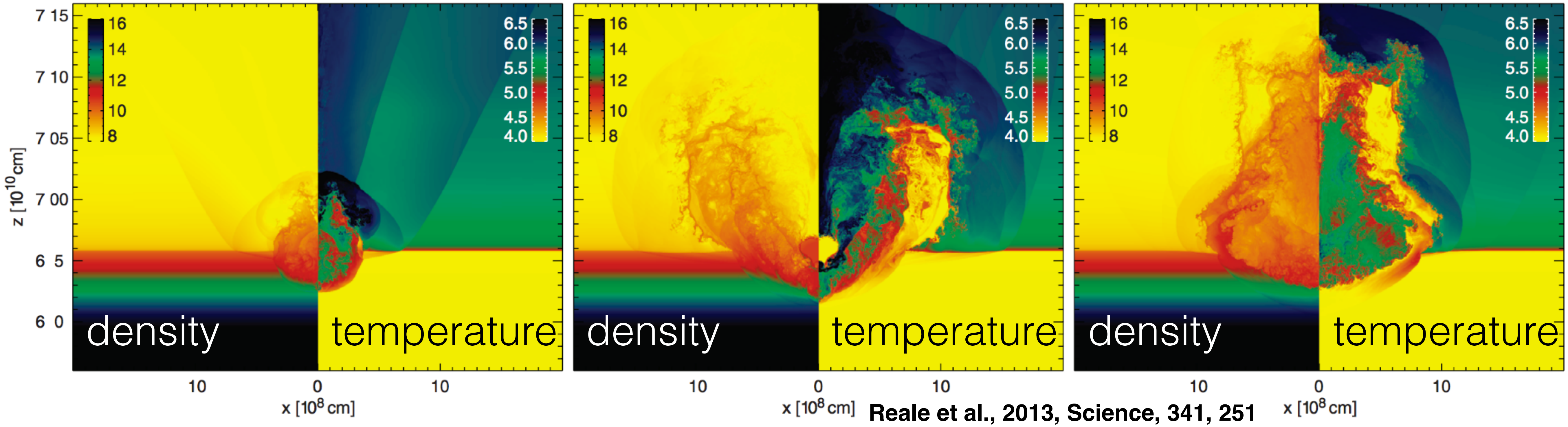

Reale et al., 2013, Science, 341, 251

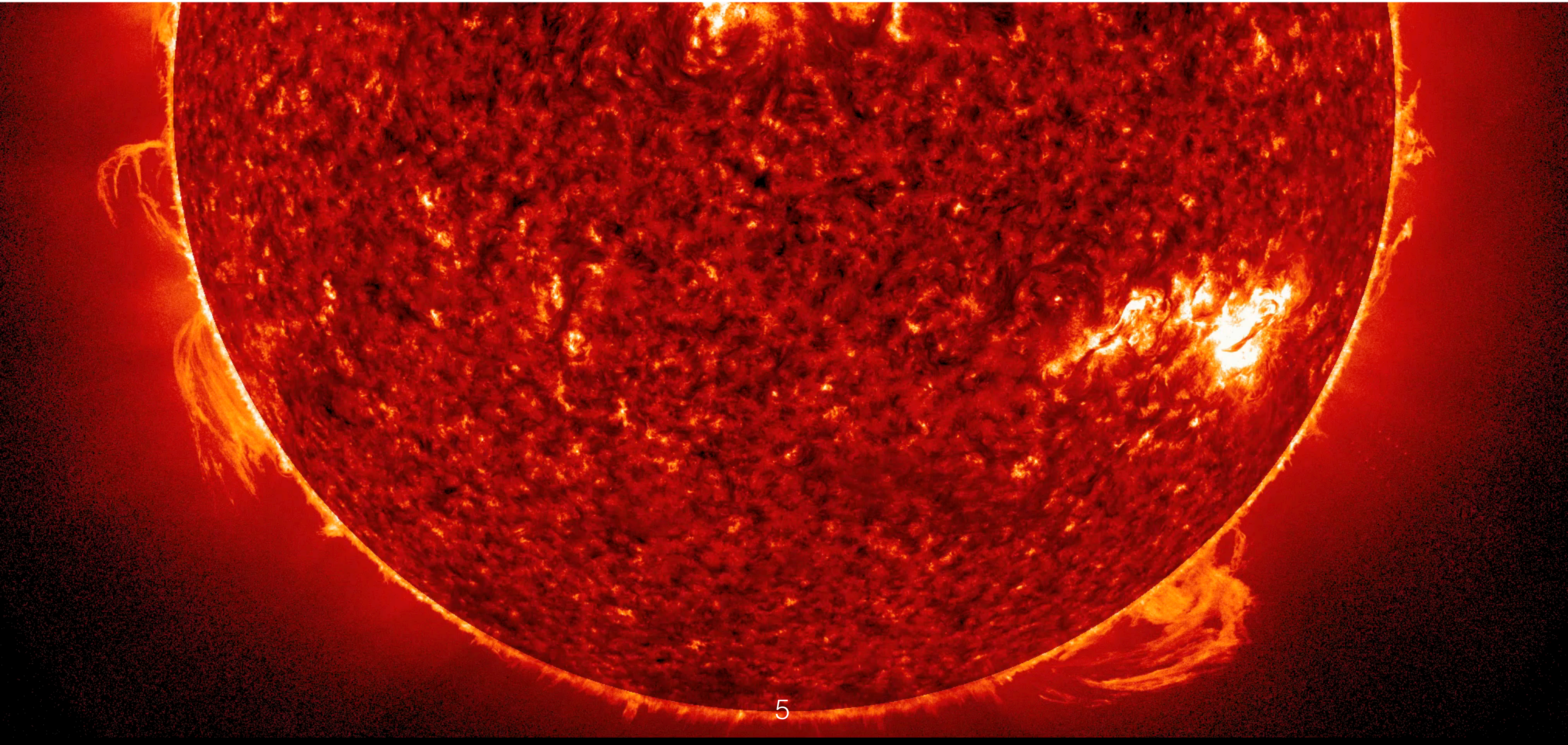

Coronal rain in SDO/AIA He 304 Å

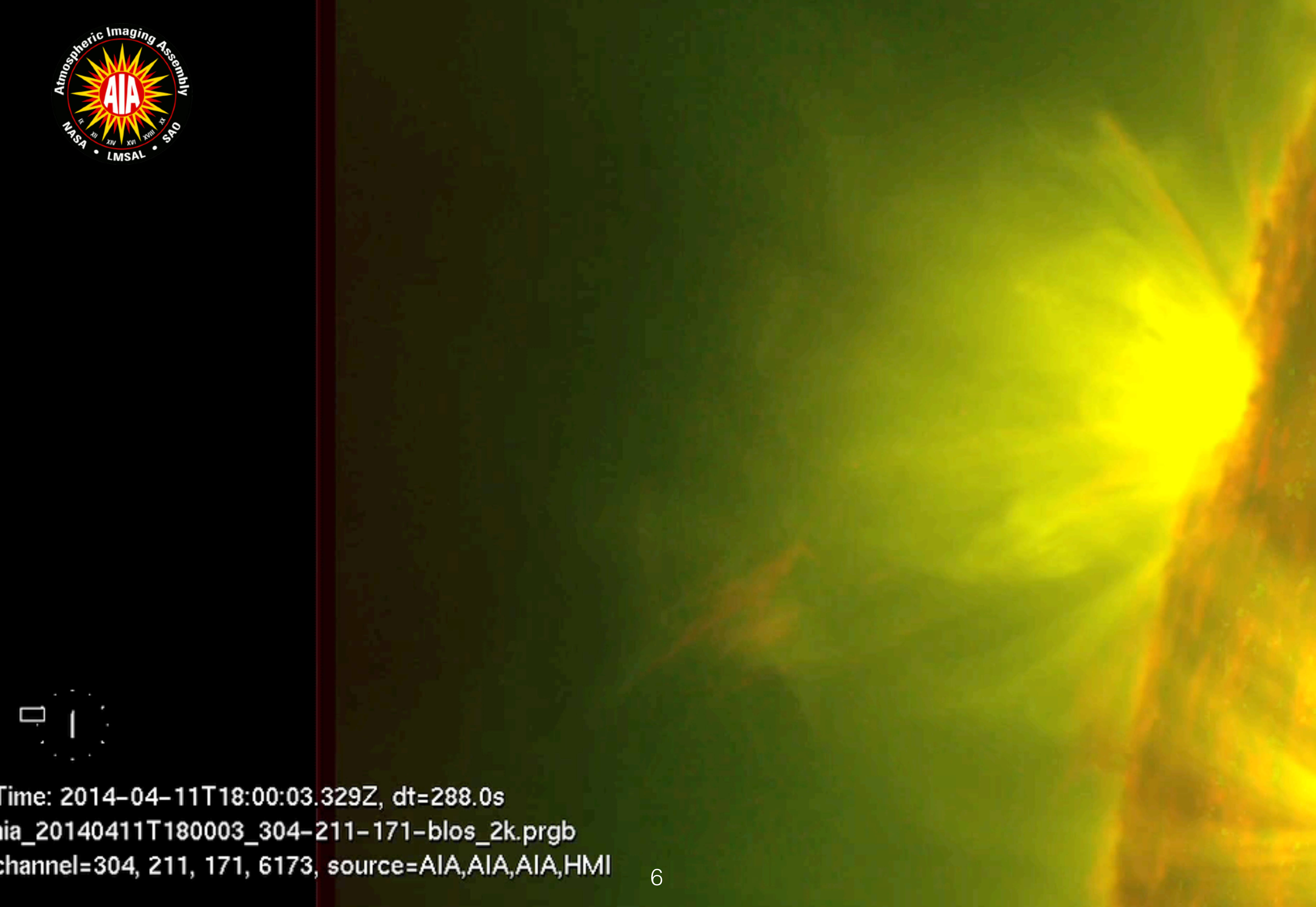

SDO's main goal is to understand, driving toward a predictive capability, the solar variations that influence life on Earth and humanity's technological systems.

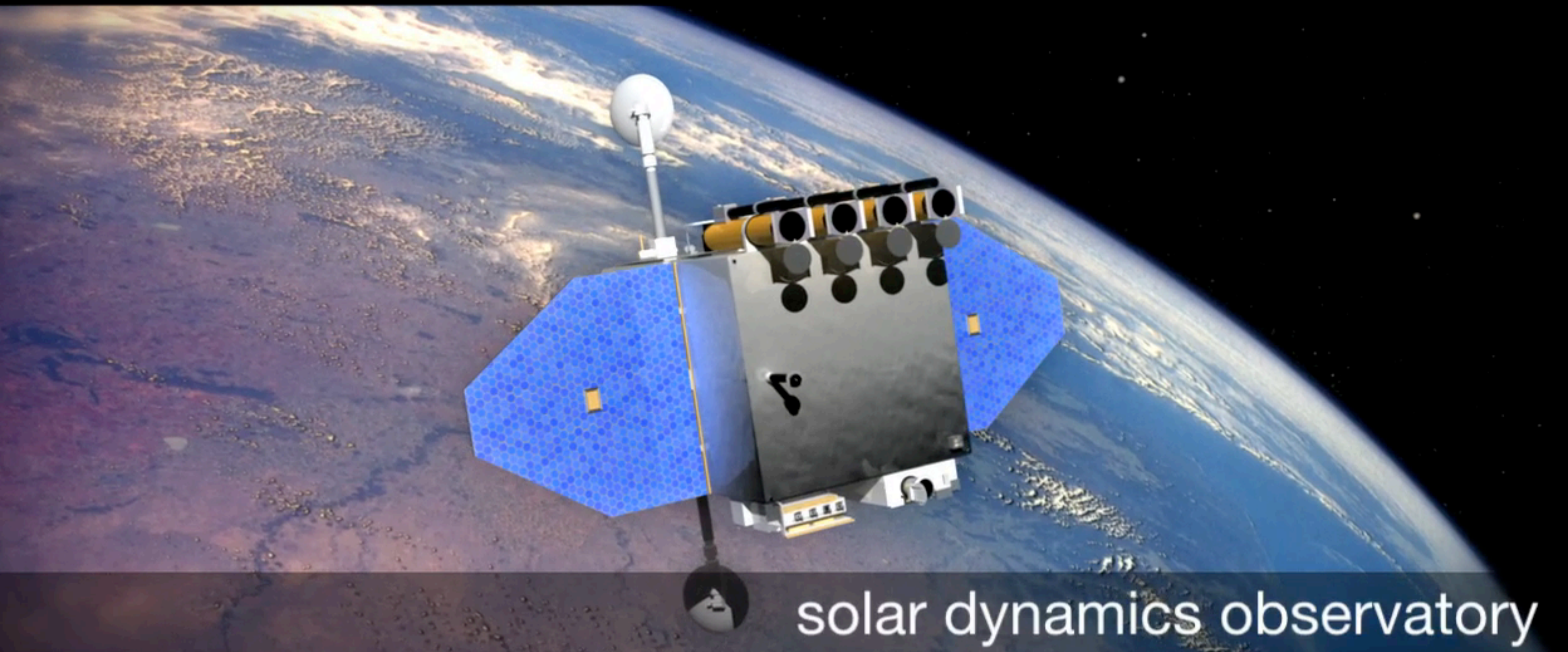

SDO images the sun's surface, atmosphere and interior.
The mission generates 2 terabytes worth of science data everyday.

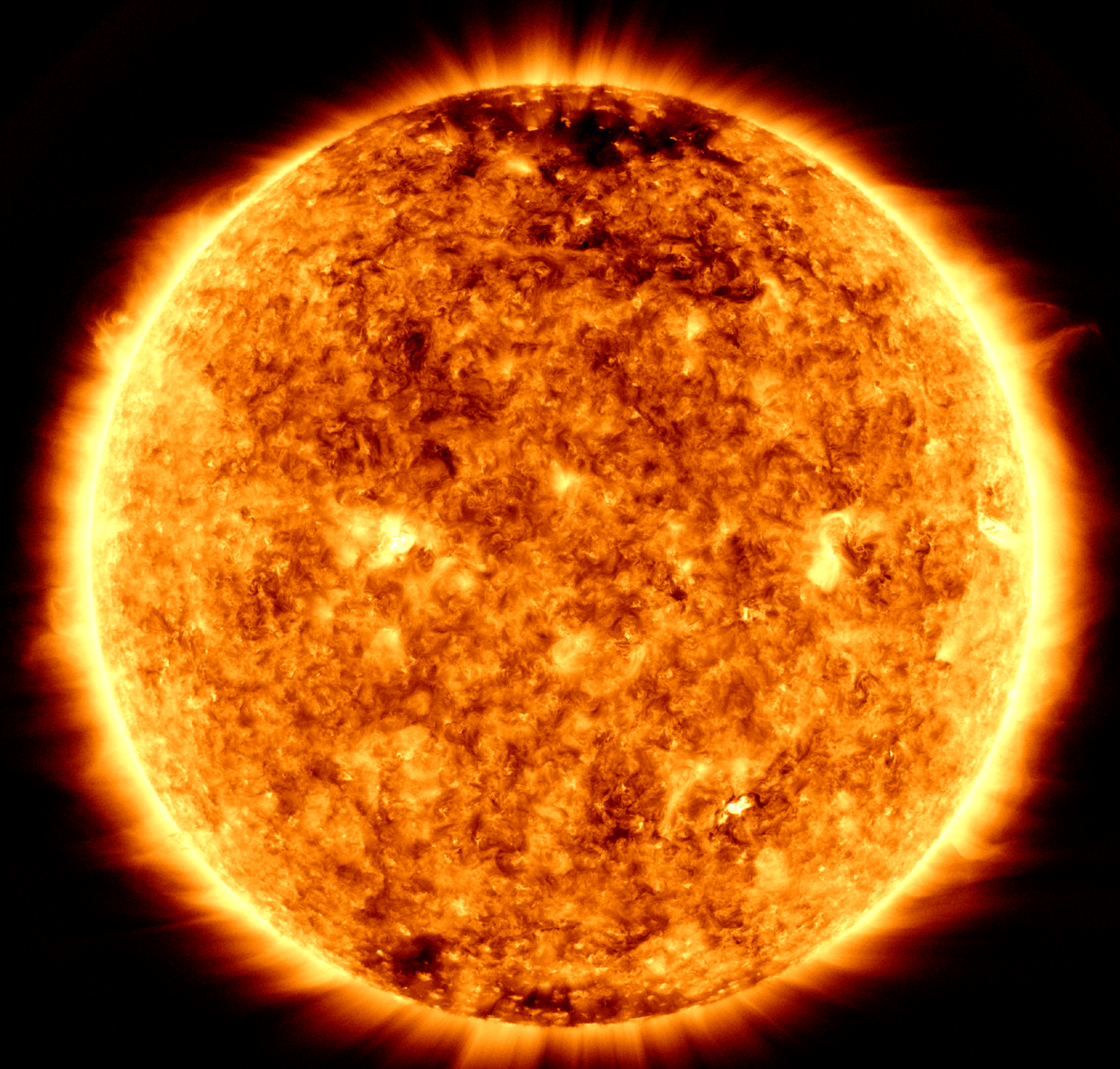

#200,000,000 from SDO/AIA on Nov 5th 2019

NASA SDO Data: A treasure trove of information

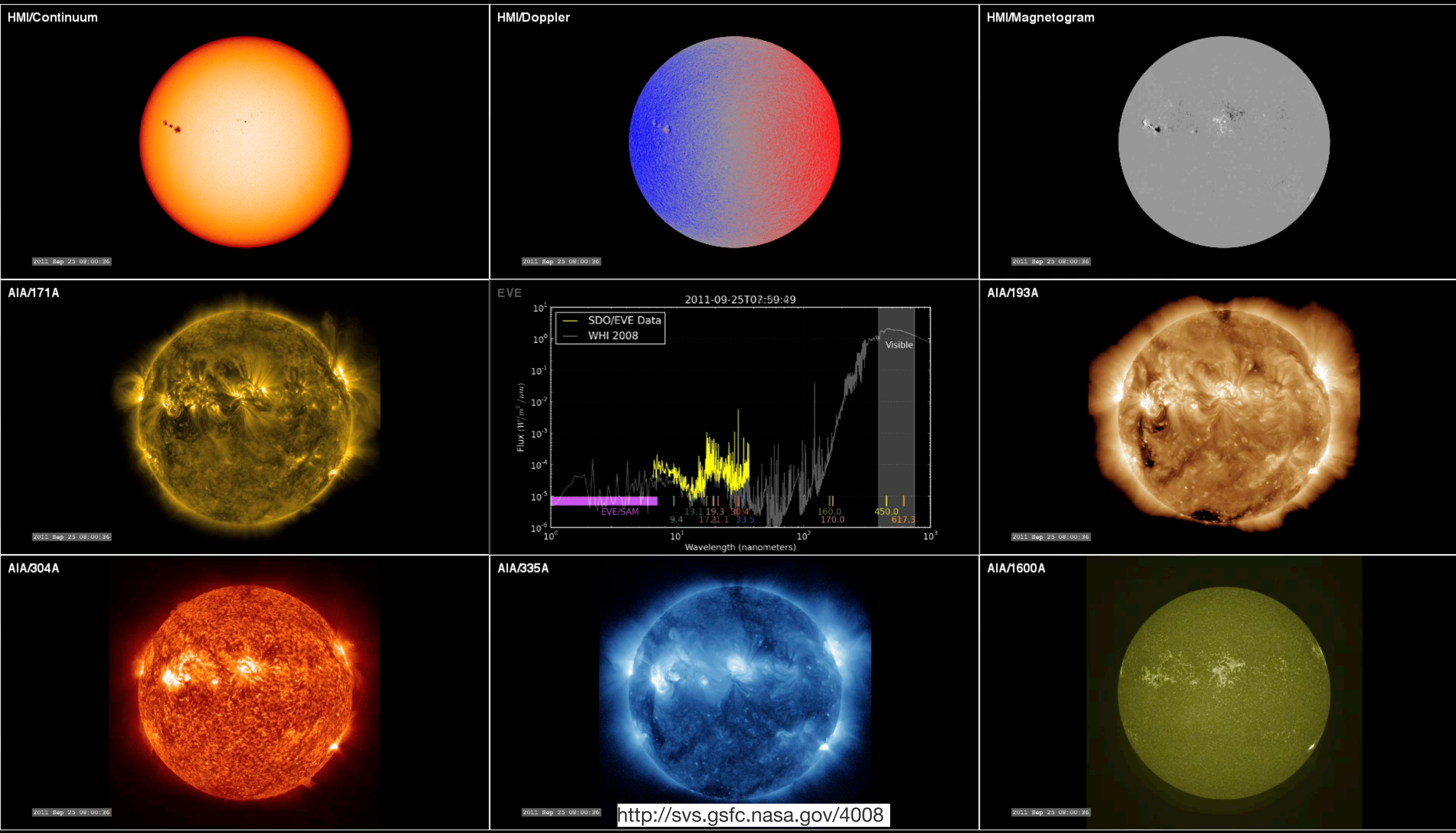

http://svs.gsfc.nasa.gov/4008

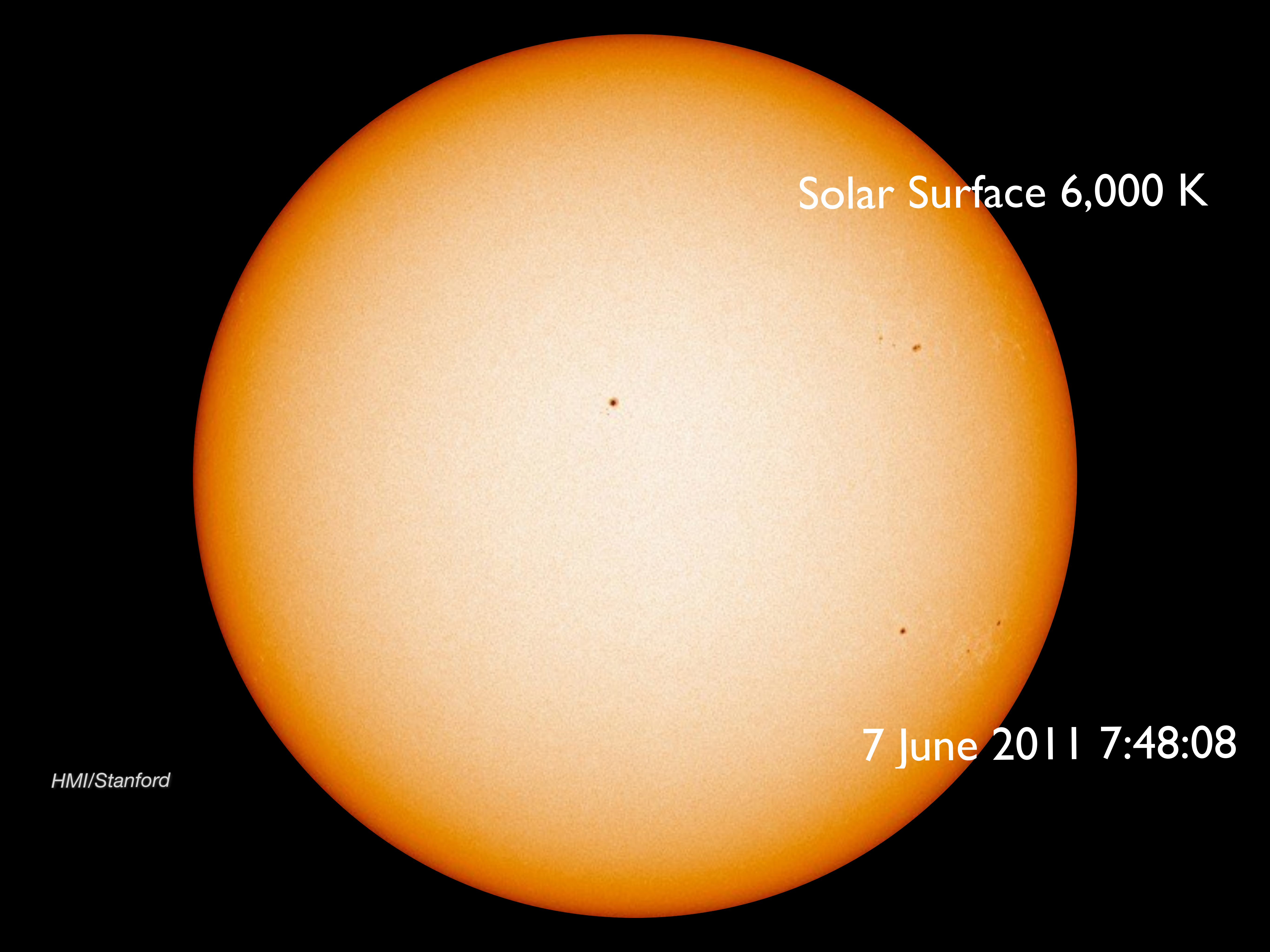
Solar Surface 6,000 K
7 June 2011 7:48:08
HMI/Stanford

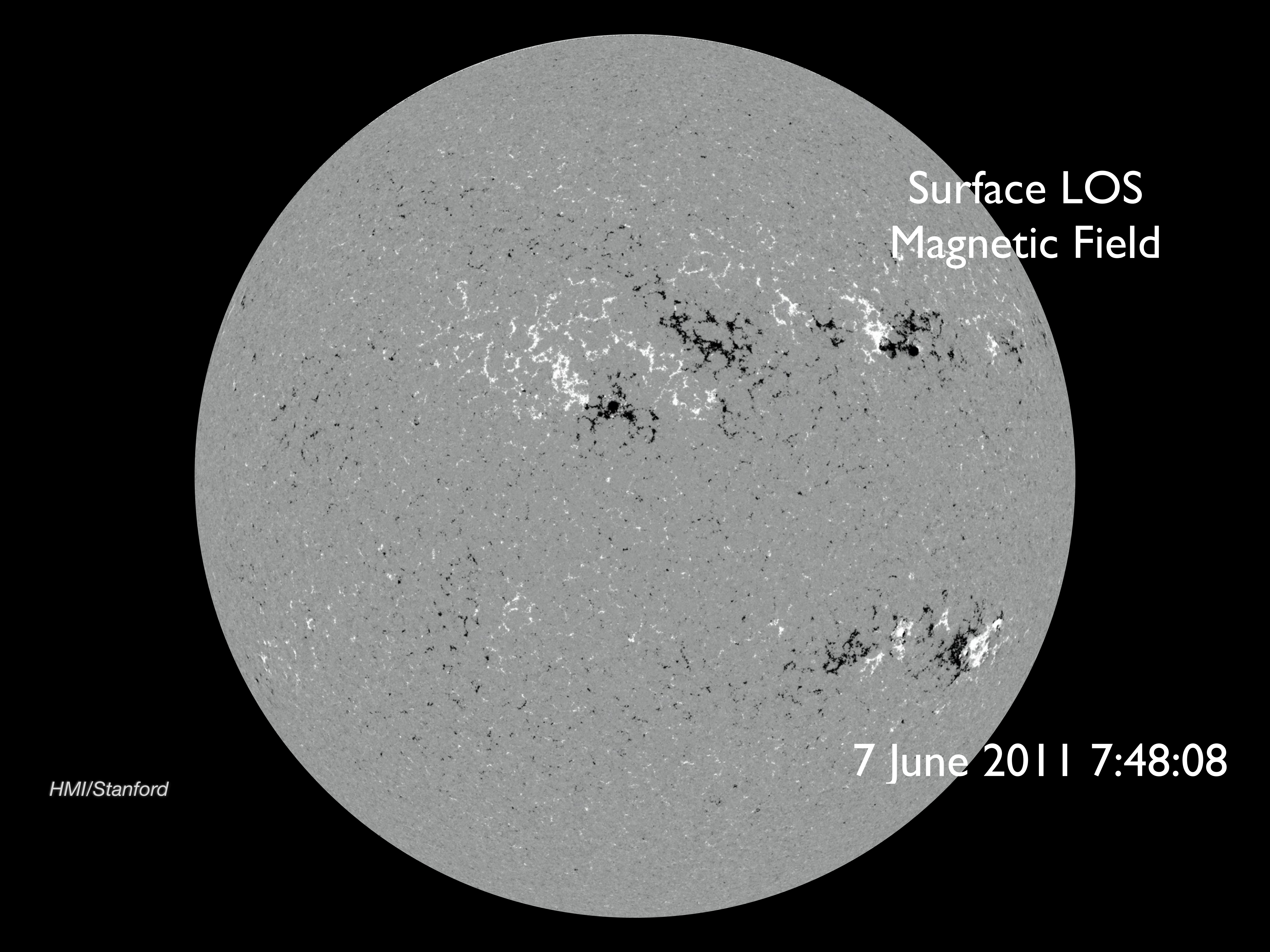
Surface LOS
Magnetic Field
7 June 2011 7:48:08
HMI/Stanford

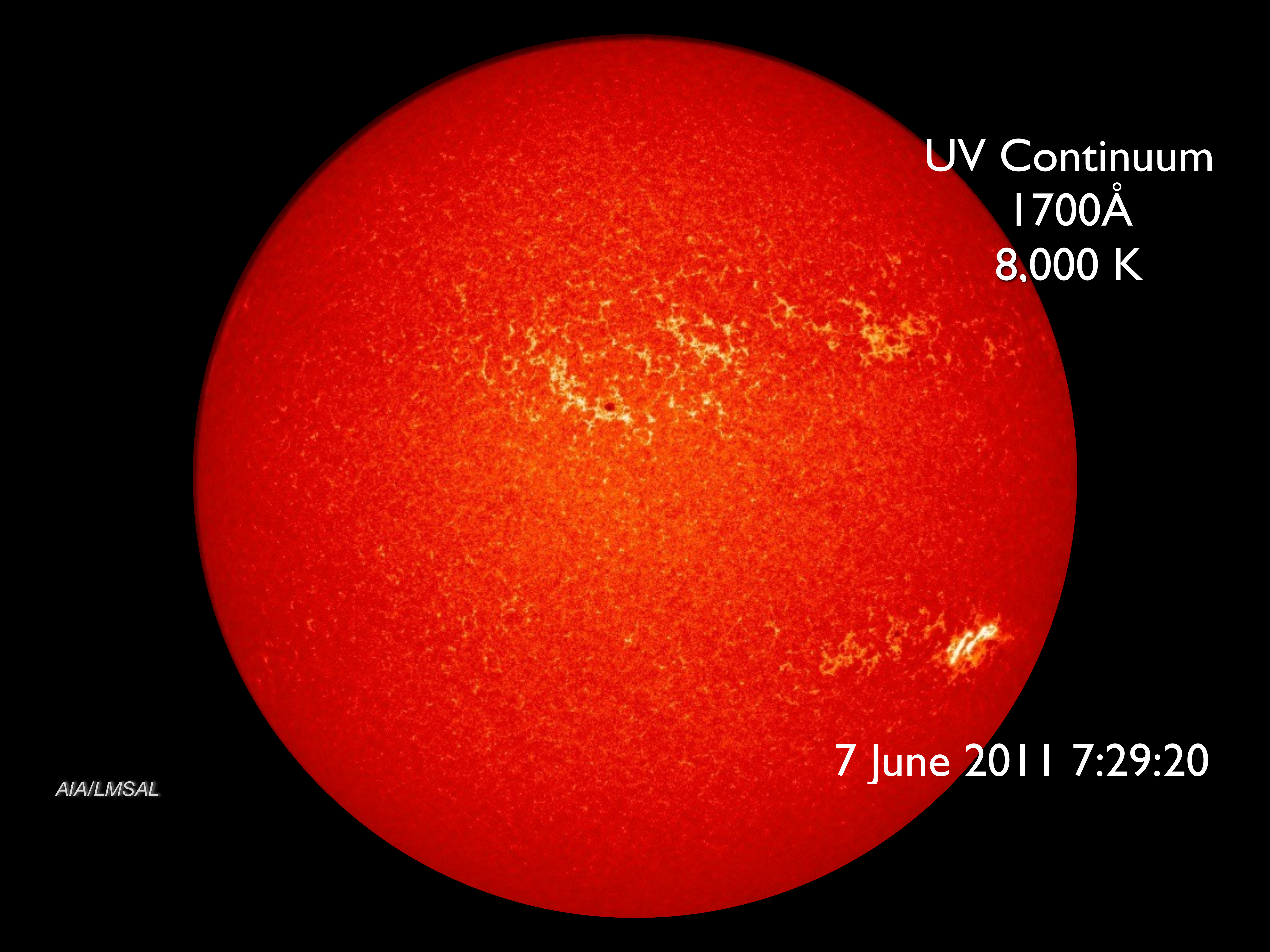
UV Continuum
1700Å
8,000 K
7 June 2011 7:29:20
AIA/LMSAL

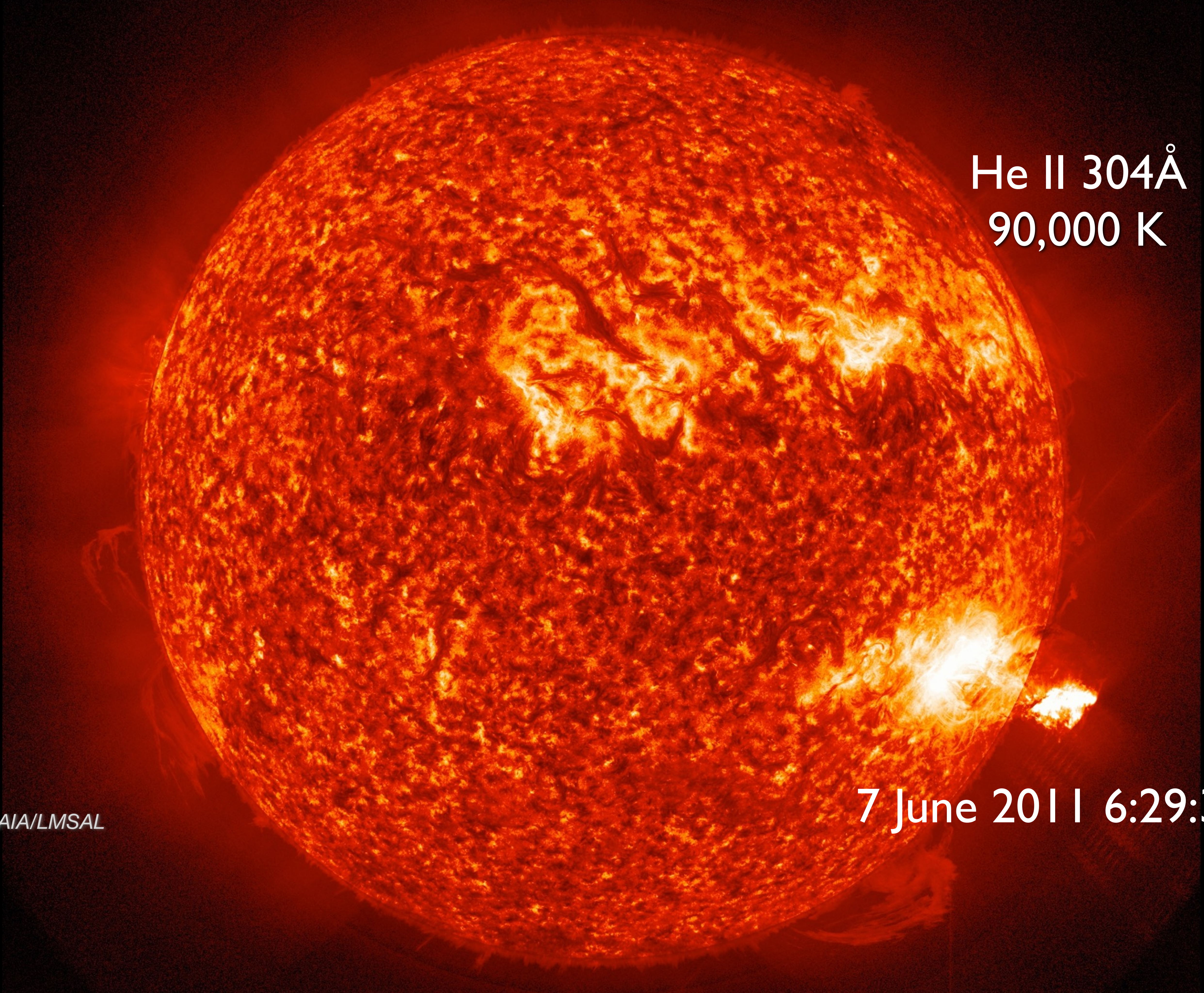
He II 304Å
90,000 K
7 June 2011 6:29:33
AIA/LMSAL

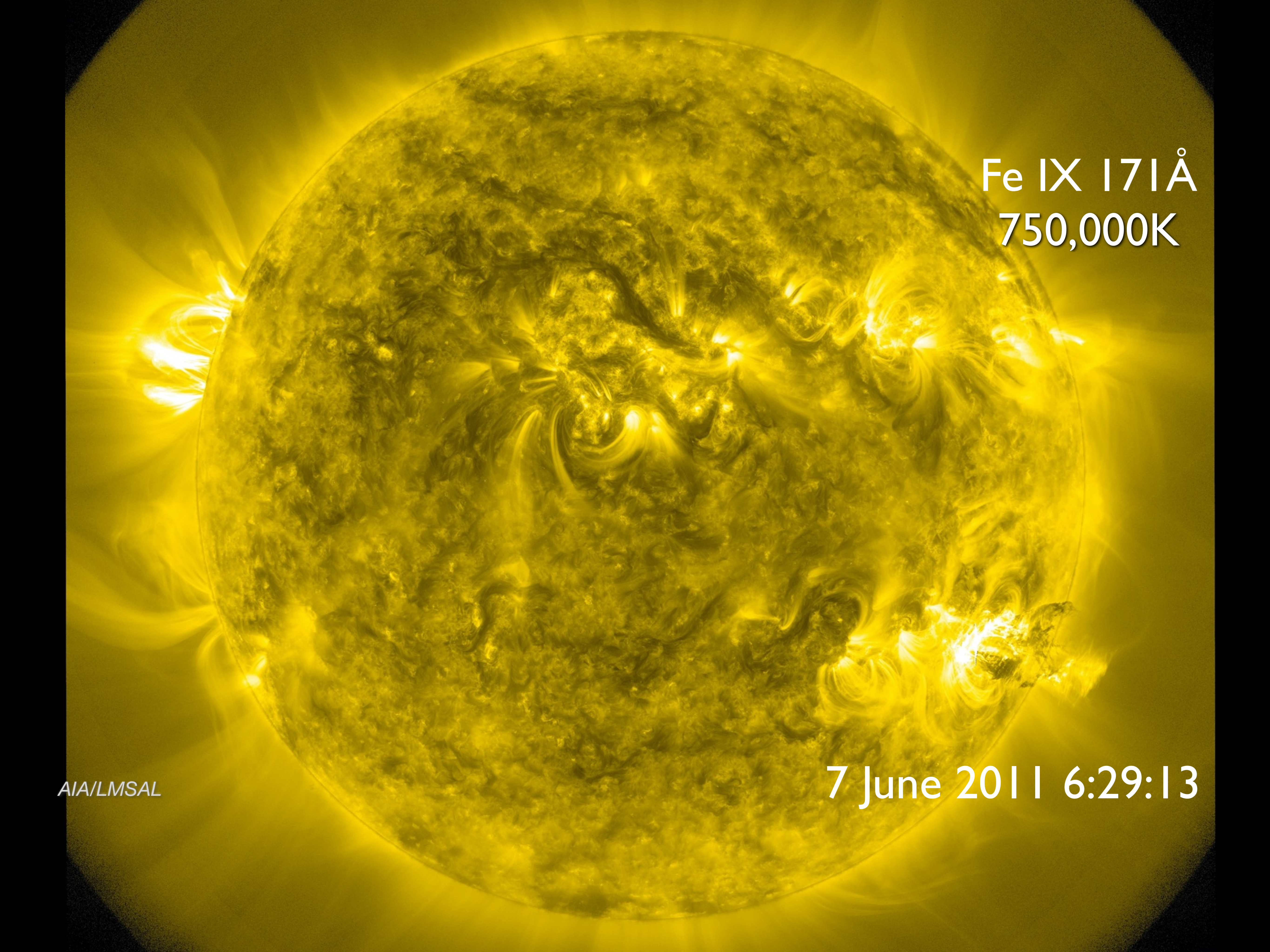
Fe IX 171Å
750,000K
7 June 2011 6:29:13
AIA/LMSAL

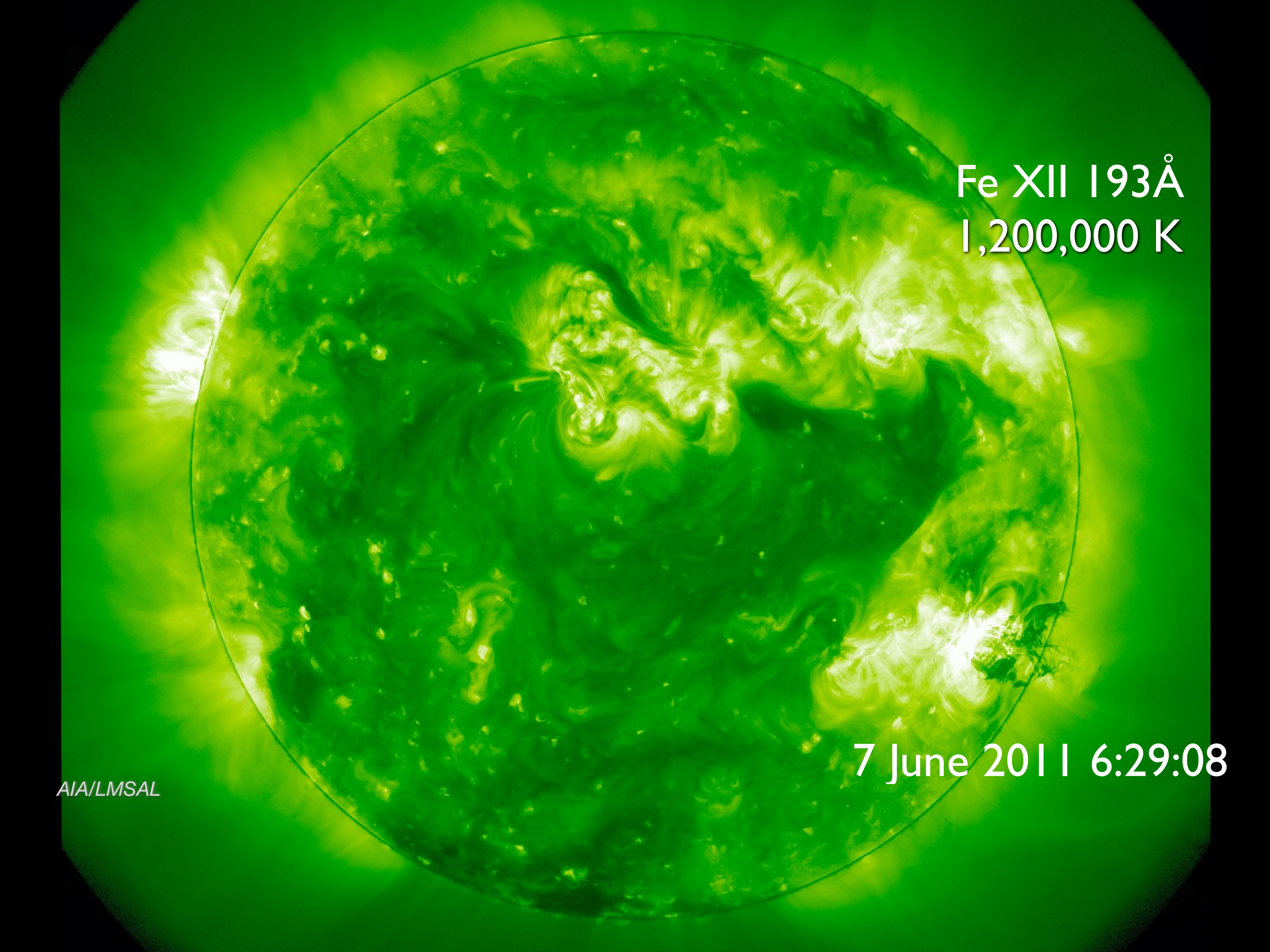
Fe XII 193Å
1,200,000 K
7 June 2011 6:29:08
AIA/LMSAL

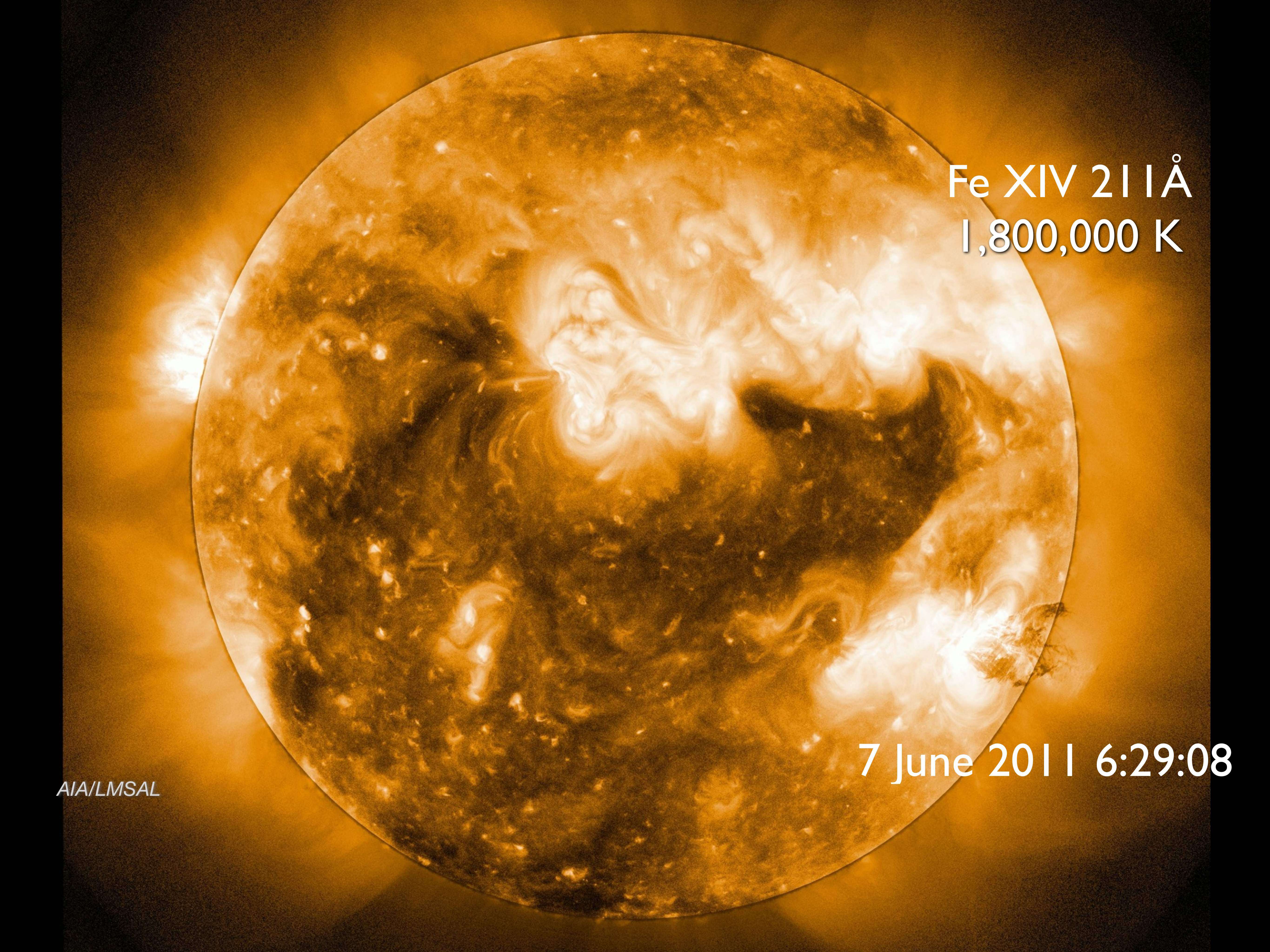
Fe XIV 211Å
1,800,000 K
7 June 2011 6:29:08
AIA/LMSAL

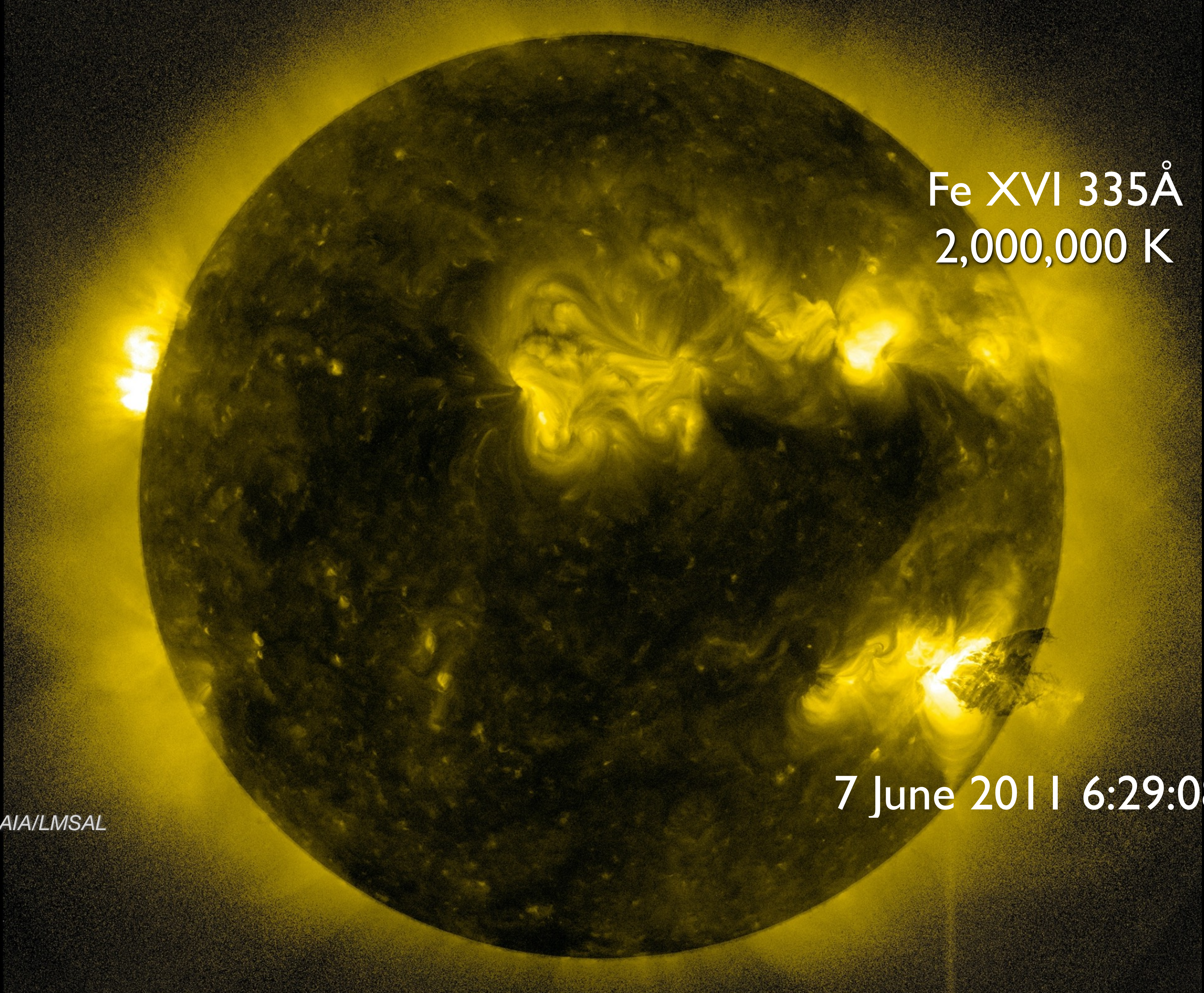
Fe XVI 335Å
2,000,000 K
7 June 2011 6:29:08
AIA/LMSAL

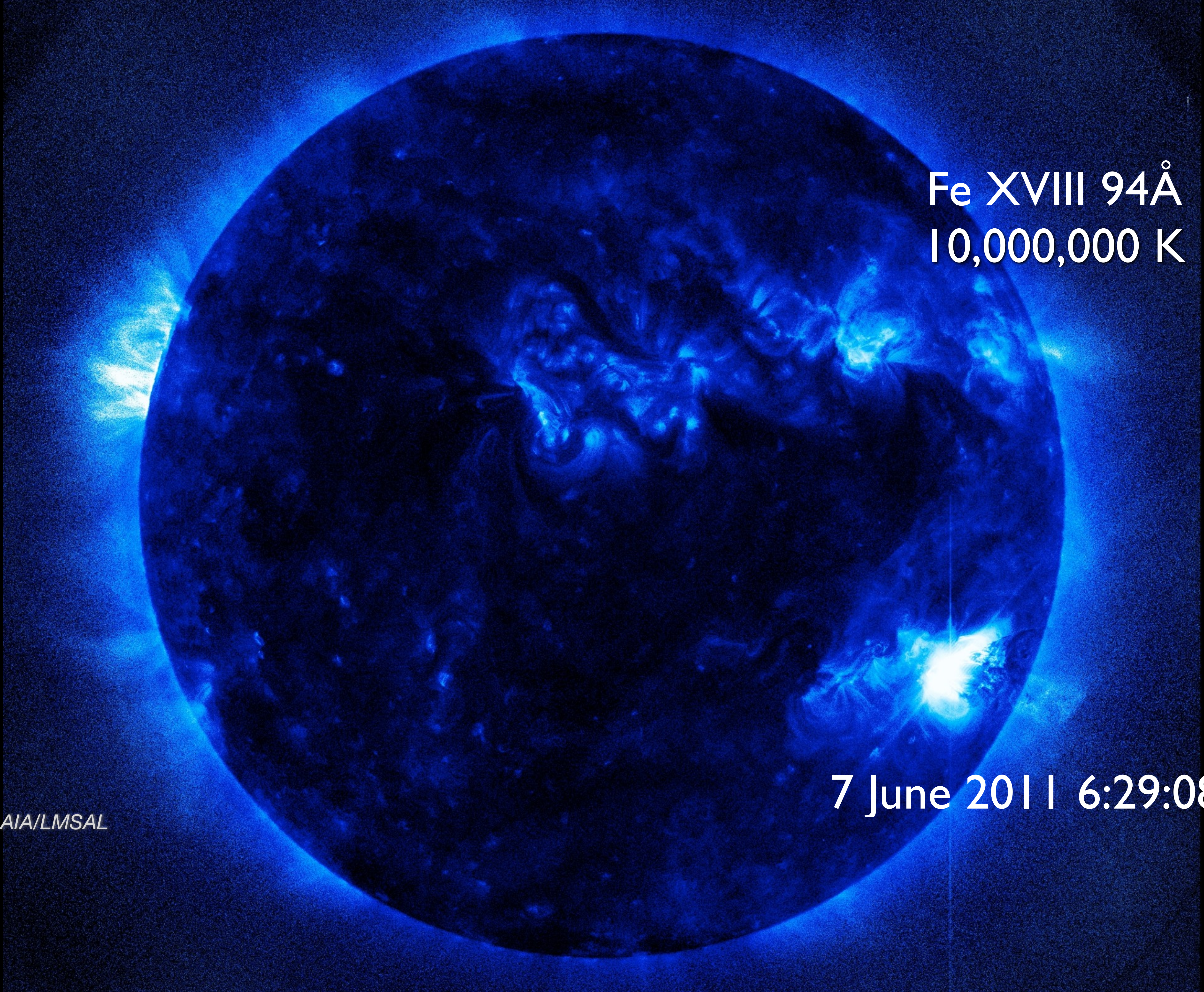
Fe XVIII 94Å
10,000,000 K
7 June 2011 6:29:08
AIA/LMSAL

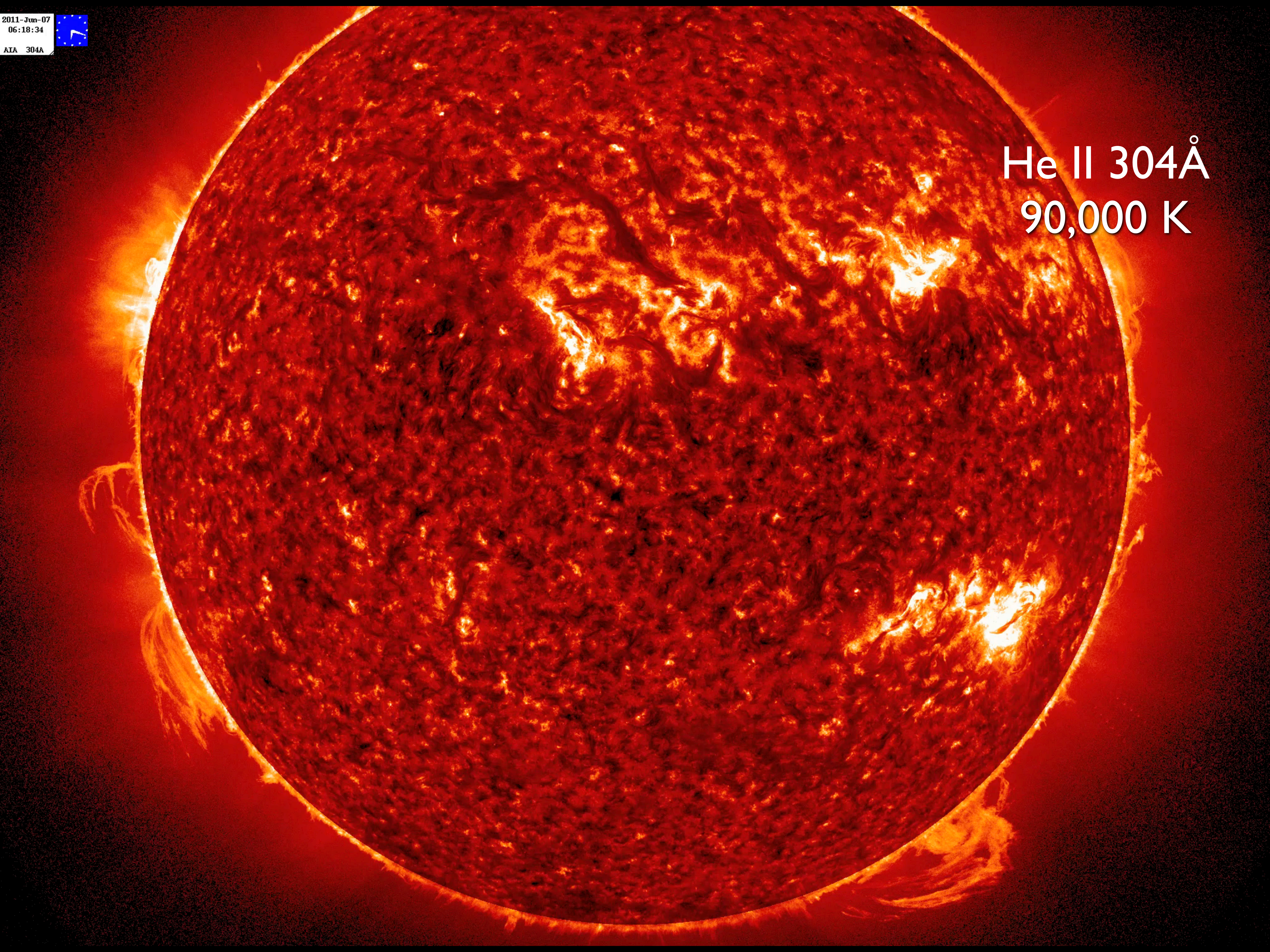
2011-Jun-07
06:18:34
AIA 304A
He II 304Å
90,000 K

Alfvén Wave Solar Model (AWSoM) van der Holst et al. 2014ApJ...782...81V

- Fully-compressible MHD equations + Alfvén wave propagation and dissipation.
- Used AIA (and STEREO) EUV images to validate the Alfvén wave heating model (as opposed to an analytical spatially-dependent heating model).
- See Alvarado-Gómez et al. (2016) for application to stellar winds of exoplanet host stars: HD 1237, HD 22049, and HD 147513.

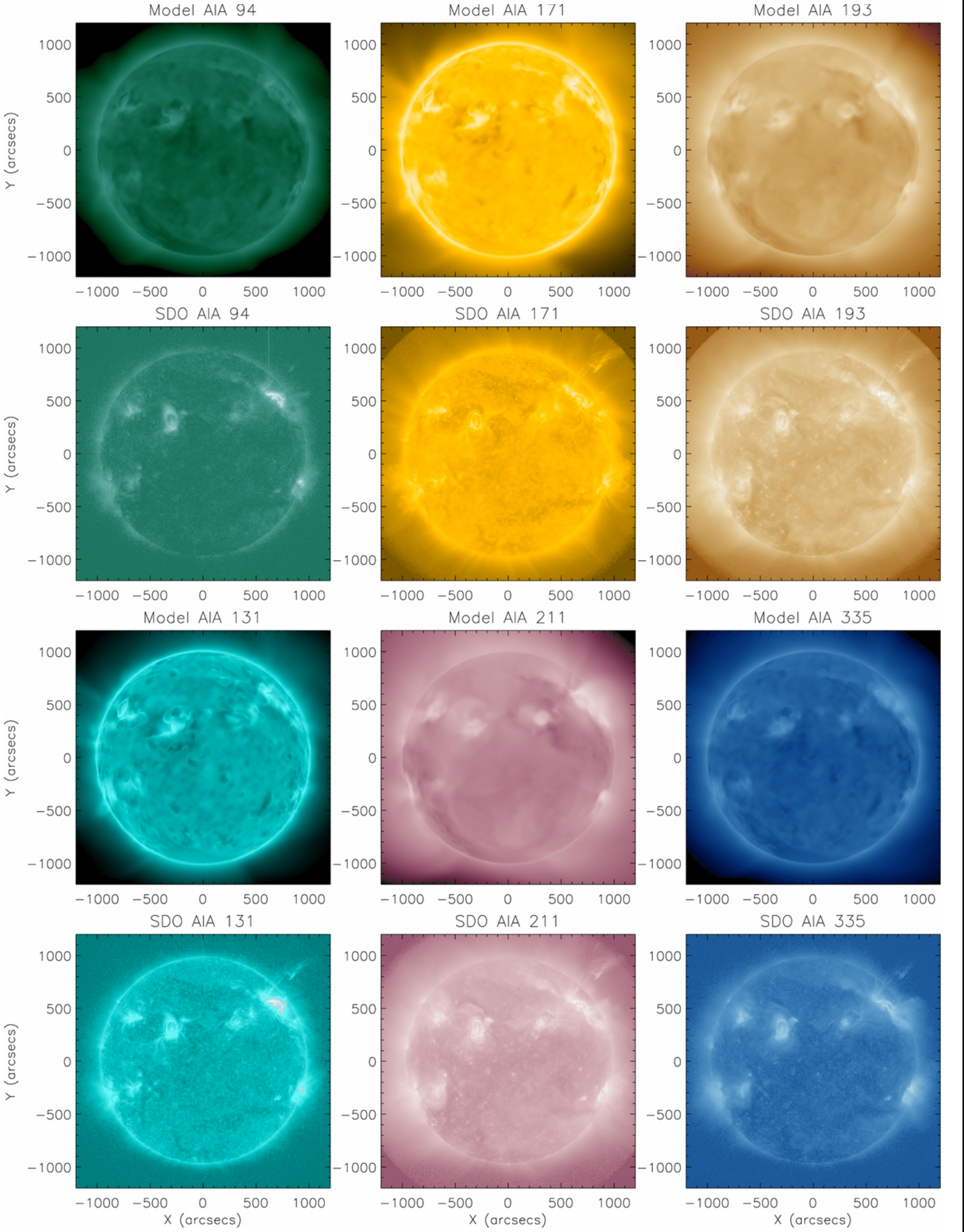

Space Weather @ Trappist-1

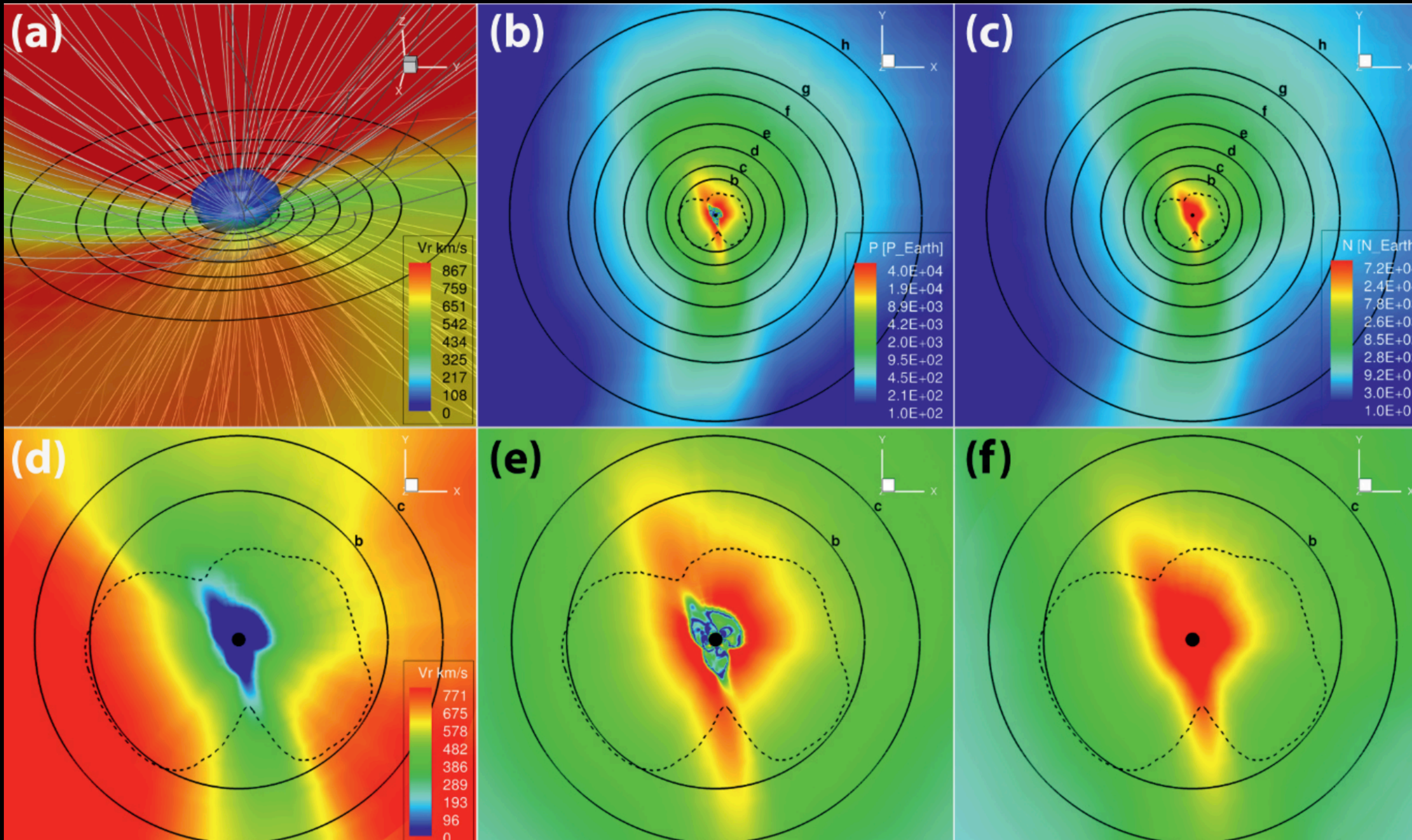

Dong + (PNAS, 2018)

Flares from Tidal Disruption Events (TDEs) around Supermassive Black Holes

Dai et al. 2018 (2018ApJ...859L..20D): In GR Radiation MHD simulations of TDEs producing super-Eddington accretion, the synthetic spectrum from the disk peaks at EUV wavelengths.

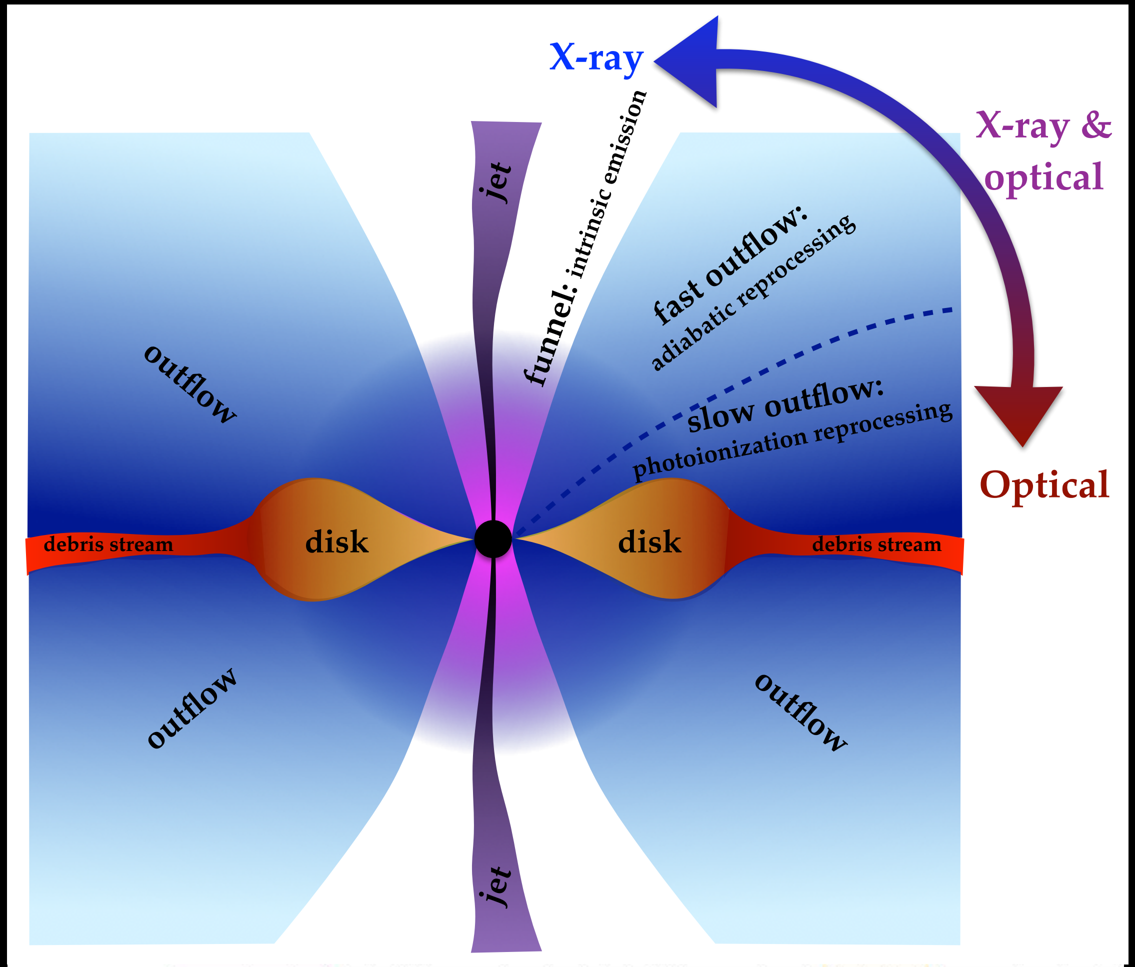

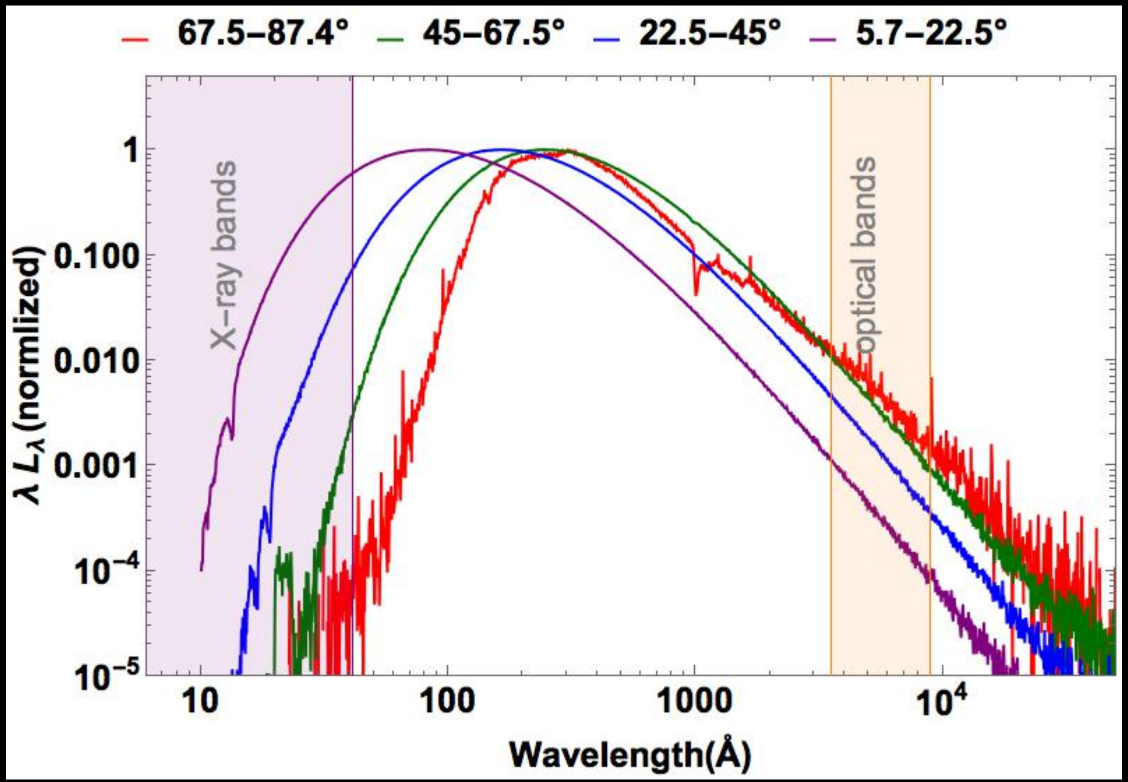

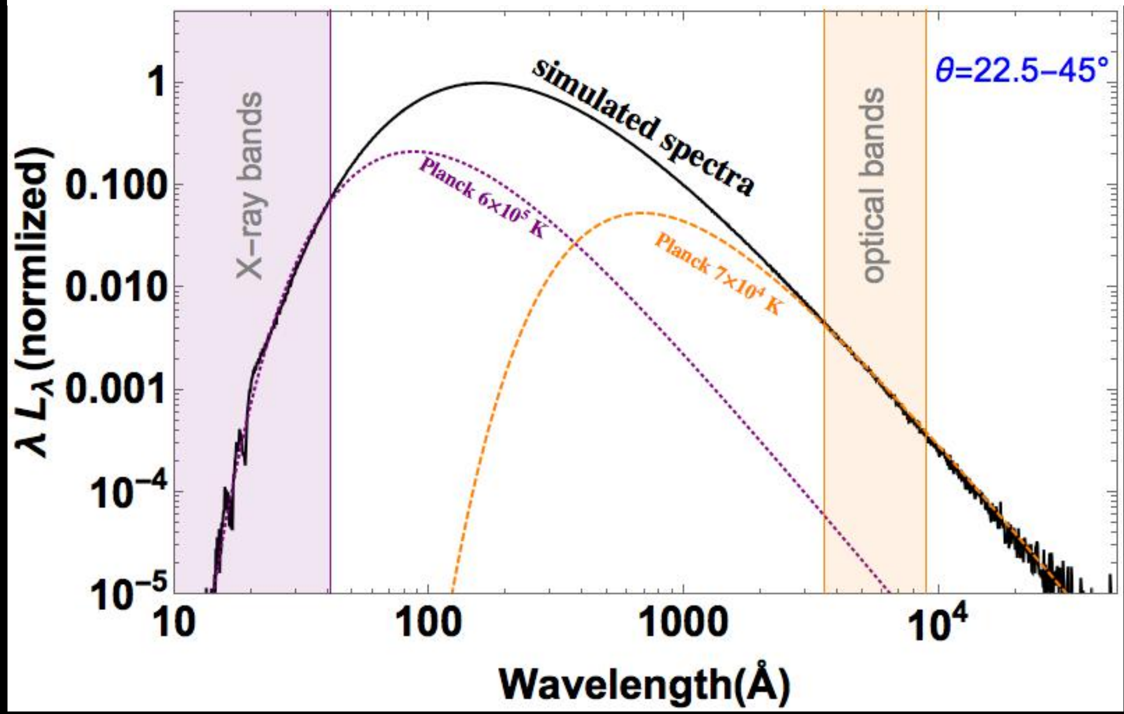

What does the SDO/Atmospheric Imaging Assembly image?

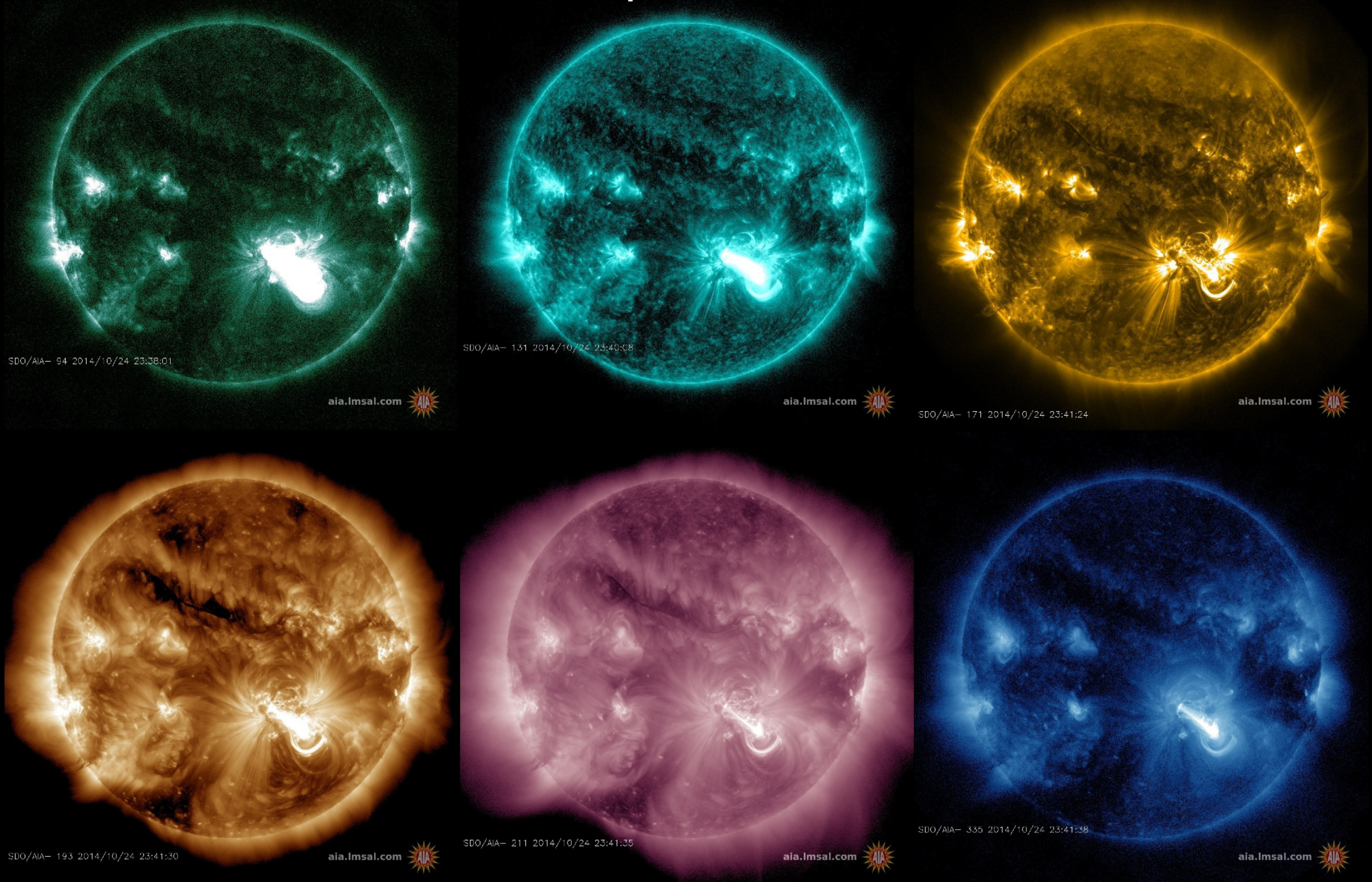

Major EUV Lines in SDO/AIA passbands

Table 1. Predicted AIA count rates.

	Ion	λ	T_p^a	Fraction of total emission			
		Å	K	CH	QS	AR	FL
94 Å	Mg VIII	94.07	5.9	0.03	-	-	-
	Fe XX	93.78	7.0	-	-	-	0.10
	Fe XVIII	93.93	6.85	-	-	0.74	0.85
	Fe X	94.01	6.05	0.63	0.72	0.05	-
	Fe VIII	93.47	5.6	0.04	-	-	-
	Fe VIII	93.62	5.6	0.05	-	-	-
	Cont.			0.11	0.12	0.17	-
131 Å	O VI	129.87	5.45	0.04	0.05	-	-
	Fe XXIII	132.91	7.15	-	-	-	0.07
	Fe XXI	128.75	7.05	-	-	-	0.83
	Fe VIII	130.94	5.6	0.30	0.25	0.09	-
	Fe VIII	131.24	5.6	0.39	0.33	0.13	-
	Cont.			0.11	0.20	0.54	0.04
171 Å	Ni XIV	171.37	6.35	-	-	0.04	-
	Fe X	174.53	6.05	-	0.03	-	-
	Fe IX	171.07	5.85	0.95	0.92	0.80	0.54
	Cont.			-	-	-	0.23
193 Å	O V	192.90	5.35	0.03	-	-	-
	Ca XVII	192.85	6.75	-	-	-	0.08
	Ca XIV	193.87	6.55	-	-	0.04	-
	Fe XXIV	192.03	7.25	-	-	-	0.81
	Fe XII	195.12	6.2	0.08	0.18	0.17	-
	Fe XII	193.51	6.2	0.09	0.19	0.17	-
	Fe XII	192.39	6.2	0.04	0.09	0.08	-
	Fe XI	188.23	6.15	0.09	0.10	0.04	-
	Fe XI	192.83	6.15	0.05	0.06	-	-
	Fe XI	188.30	6.15	0.04	0.04	-	-
	Fe X	190.04	6.05	0.06	0.04	-	-
	Fe IX	189.94	5.85	0.06	-	-	-
	Fe IX	188.50	5.85	0.07	-	-	-
	Cont.			-	-	0.05	0.04
211 Å	Cr IX	210.61	5.95	0.07	-	-	-
	Ca XVI	208.60	6.7	-	-	-	0.09
	Fe XVII	204.67	6.6	-	-	-	0.07
	Fe XIV	211.32	6.3	-	0.13	0.39	0.12
	Fe XIII	202.04	6.25	-	0.05	-	-
	Fe XIII	203.83	6.25	-	-	0.07	-
	Fe XIII	209.62	6.25	-	0.05	0.05	-
	Fe XI	209.78	6.15	0.11	0.12	-	-
	Fe X	207.45	6.05	0.05	0.03	-	-
	Ni XI	207.92	6.1	0.03	-	-	-
	Cont.			0.08	0.04	0.07	0.41
304 Å	He II	303.786	4.7	0.33	0.32	0.27	0.29
	He II	303.781	4.7	0.66	0.65	0.54	0.58
	Ca XVIII	302.19	6.85	-	-	-	0.05
	Si XI	303.33	6.2	-	-	0.11	-
	Cont.			-	-	-	-
335 Å	Al X	332.79	6.1	0.05	0.11	-	-
	Mg VIII	335.23	5.9	0.11	0.06	-	-
	Mg VIII	338.98	5.9	0.11	0.06	-	-
	Si IX	341.95	6.05	0.03	0.03	-	-
	Si VIII	319.84	5.95	0.04	-	-	-
	Fe XVI	335.41	6.45	-	-	0.86	0.81
	Fe XIV	334.18	6.3	-	0.04	0.04	-
	Fe X	184.54	6.05	0.13	0.15	-	-
	Cont.			0.08	0.05	-	0.06

O'Dwyer, Del Zanna, Mason & Weber (A&A 2010), using the CHIANTI atomic package

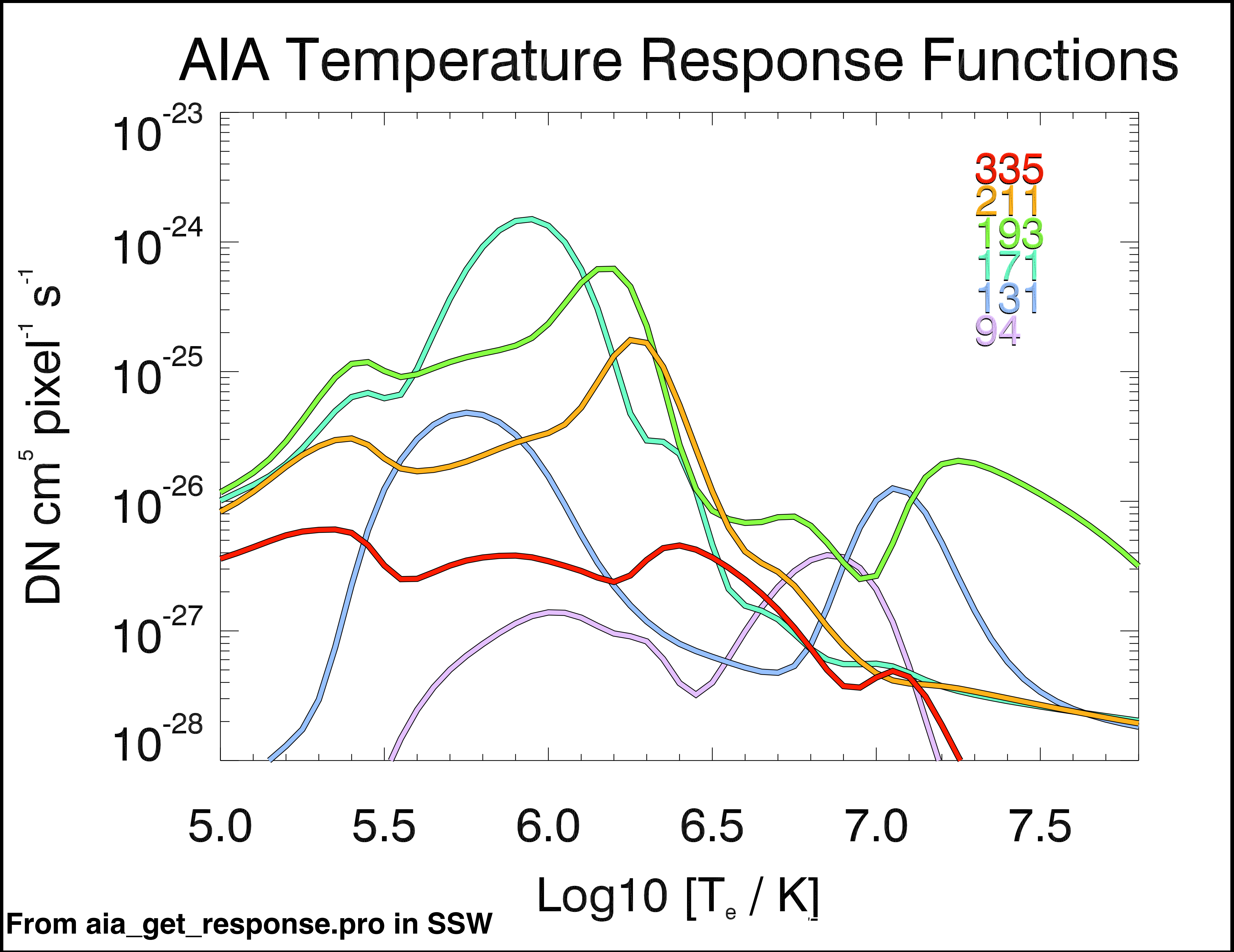

Problem Statement

$\boldsymbol{y} = \boldsymbol{K}\boldsymbol{x}$

rows of $\boldsymbol{K}$ = temp responses of AIA channels

$\boldsymbol{y}$ = AIA count rates

$\boldsymbol{x} = \boldsymbol{D}\boldsymbol{m}$, cols. of $\boldsymbol{D}$ = basis funcs

$\boldsymbol{m}$ = emission measure (EM) in temperature bins

EM @ certain temperature = line-of-sight integral of n_e^2

Sparse Solution by Basis Pursuit

In practice, measurement uncertainties imply that the equality **y** = *K***x** may not be satisfied. So our method solves the following linear program:

$$\text{minimize} \sum_j^n \mathrm{x}_j \text{ subject to } \mathcal{K}\vec{x} \leq \vec{y} + \vec{\eta},$$
$$\vec{x} \geq 0,\ \mathcal{K}\vec{x} \geq \max(\vec{y} - \vec{\eta}, 0).$$

The vector **η** is a measure of the uncertainty in the count rate and provides tolerance for the predicted counts (*K***x**) to deviate from the observed values (**y**). To enforce positive counts the lower bound is set to max(***y*-η**, 0).

Cheung et al. (2015): This method has been validated on (1) simple log-normal DEM models, (2) 3D model of quasi-steadily heated loops in a non-linear force-free field and (3) 3D MHD model of an active region with field-aligned thermal conduction.

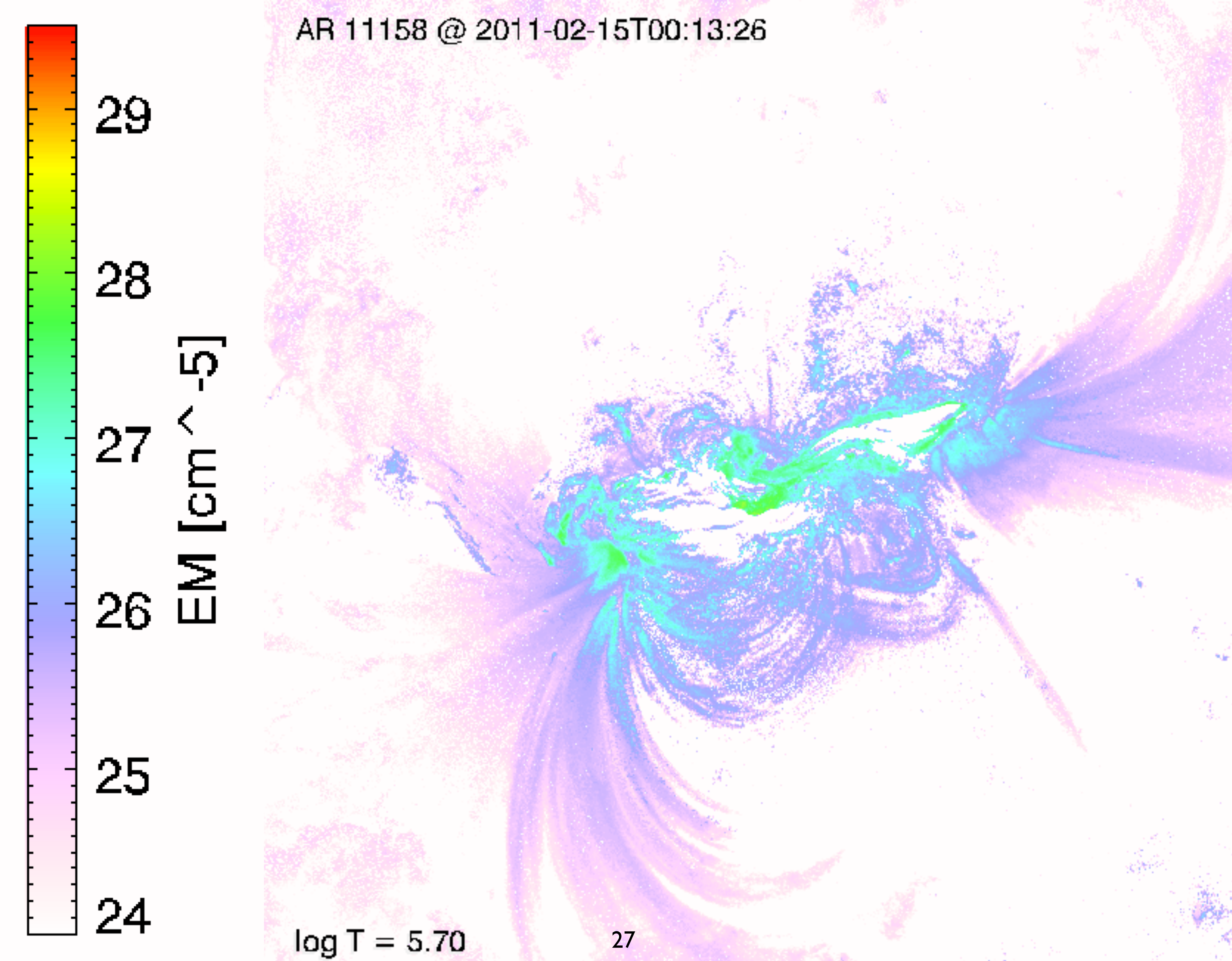
AR 11158 @ 2011-02-15T00:13:26
29
28
27
26
25
24
EM [cm ^ -5]
log T = 5.70

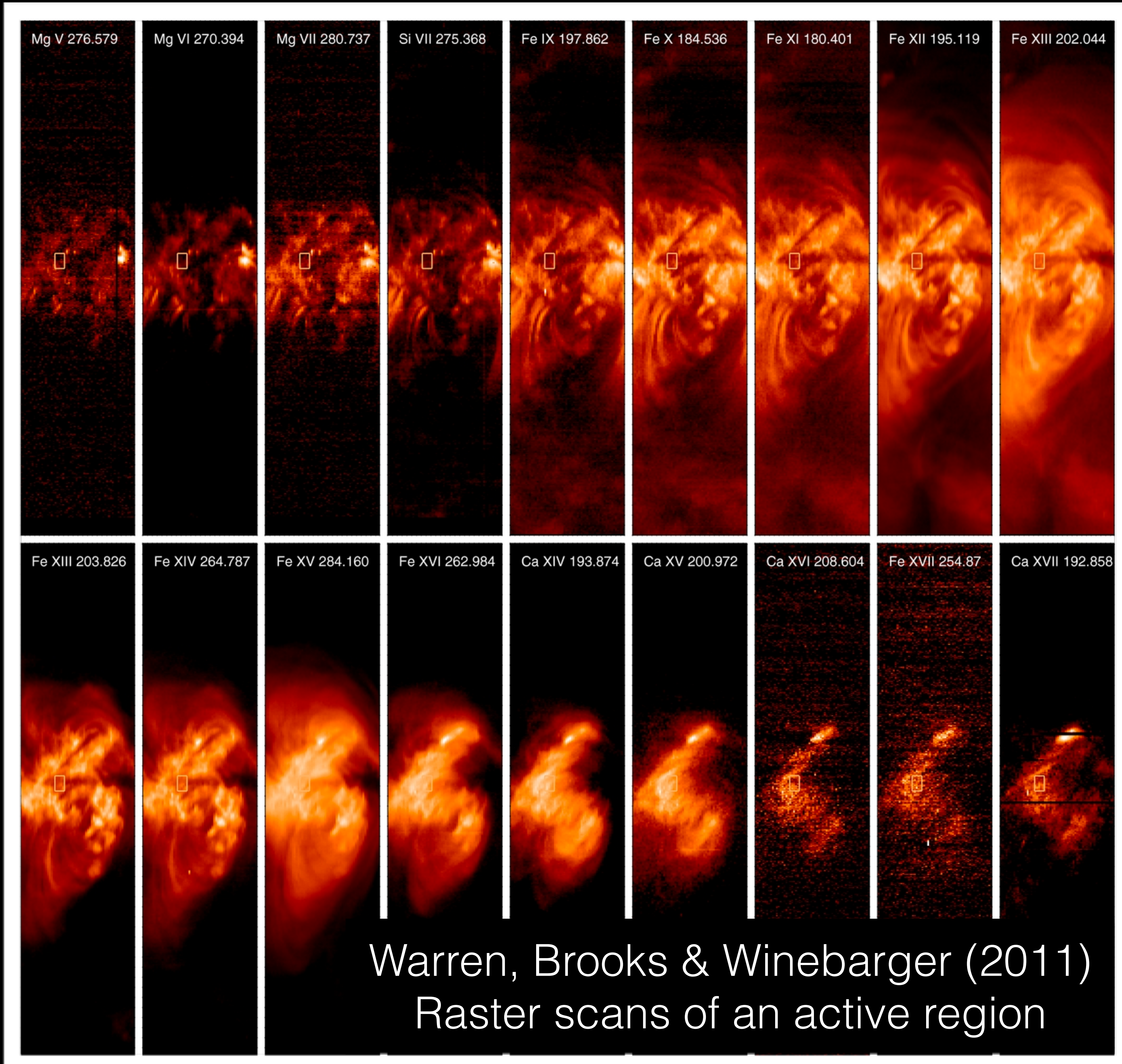

Warren, Brooks & Winebarger (2011)
Raster scans of an active region

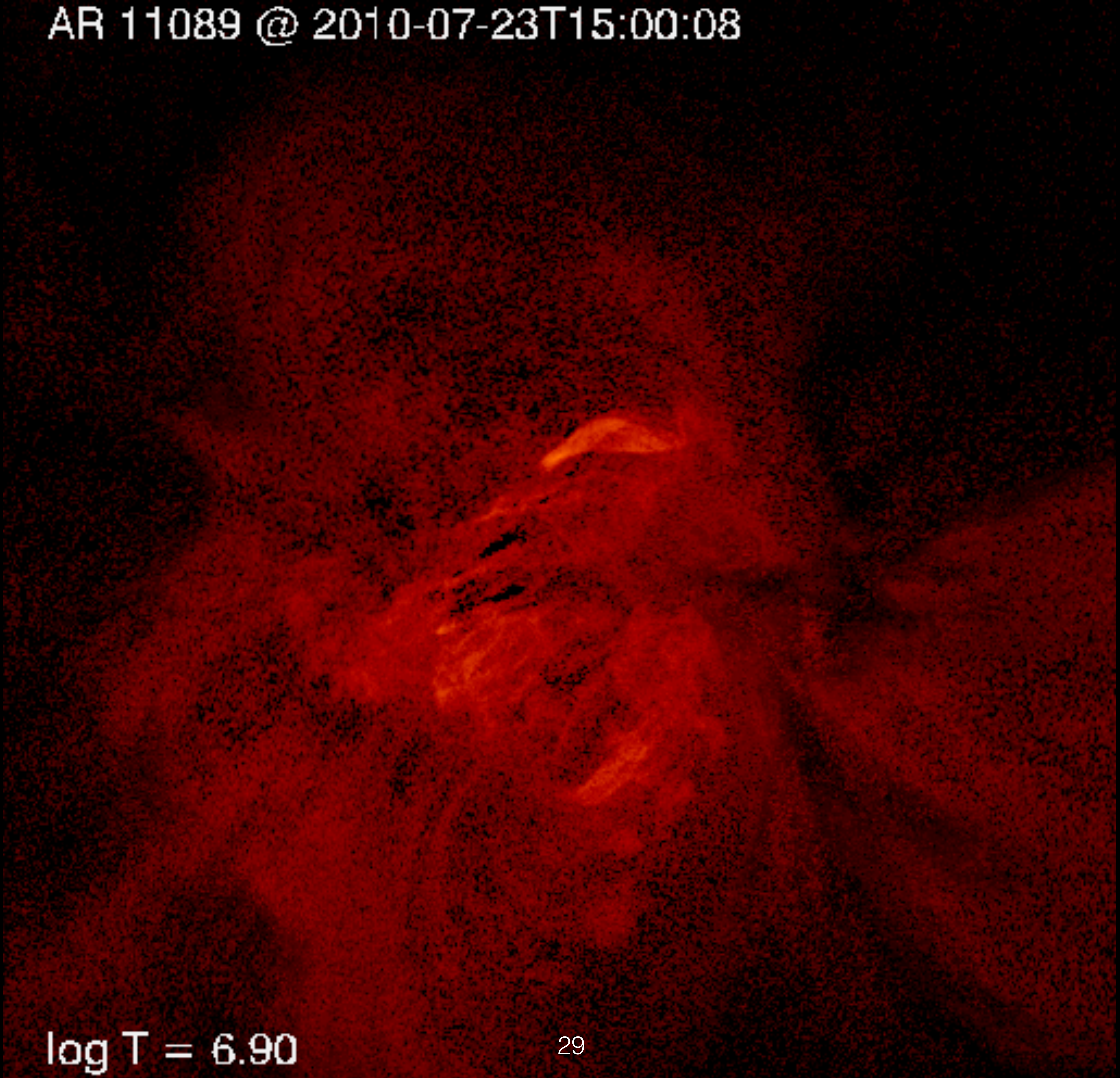
AR 11089 @ 2010-07-23T15:00:08
log T = 6.90

Validation Exercise*: AIA-XRT Cross-Comparison

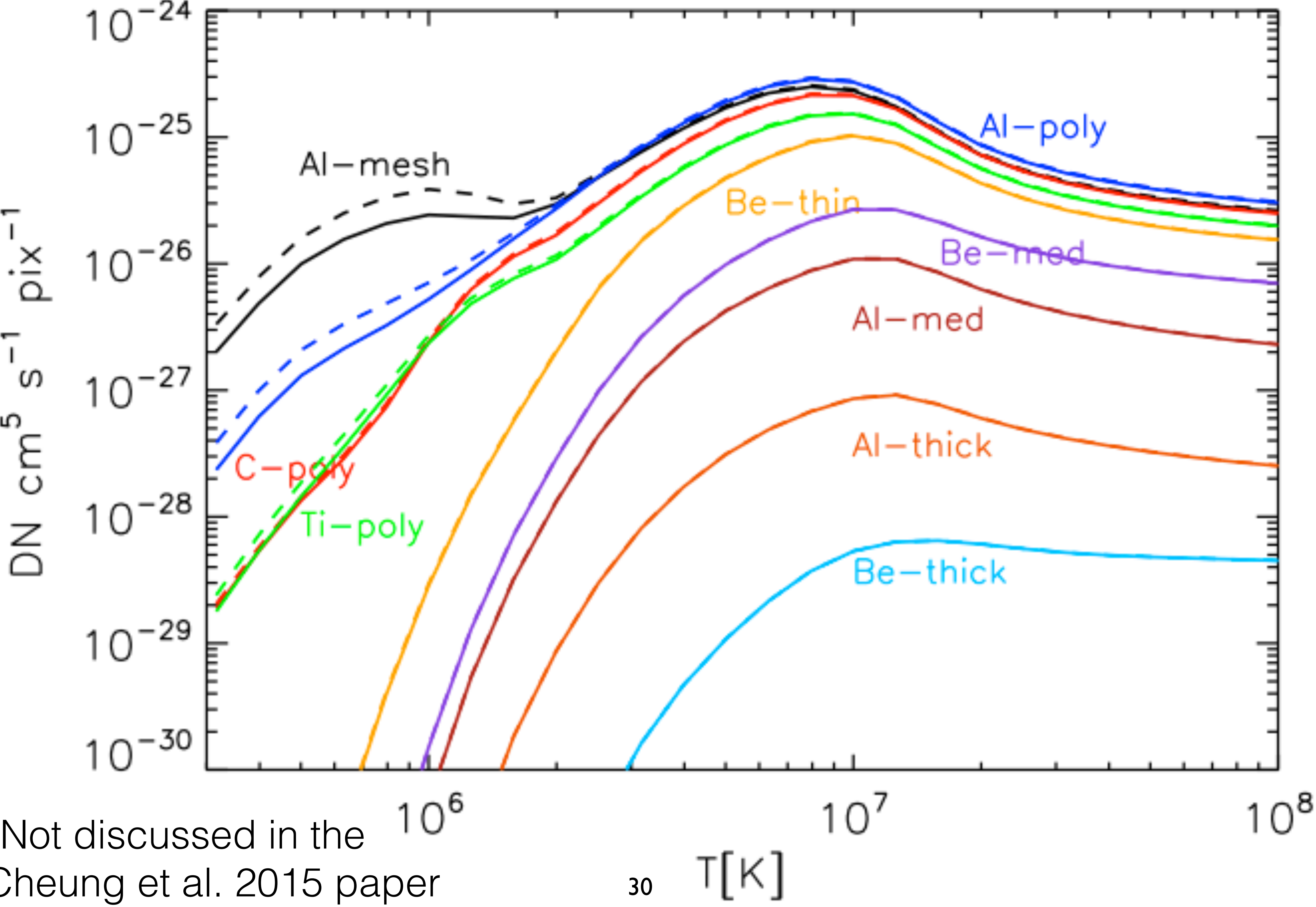

*Not discussed in the Cheung et al. 2015 paper

Hinode/XRT   AIA DEM -> Mock XRT

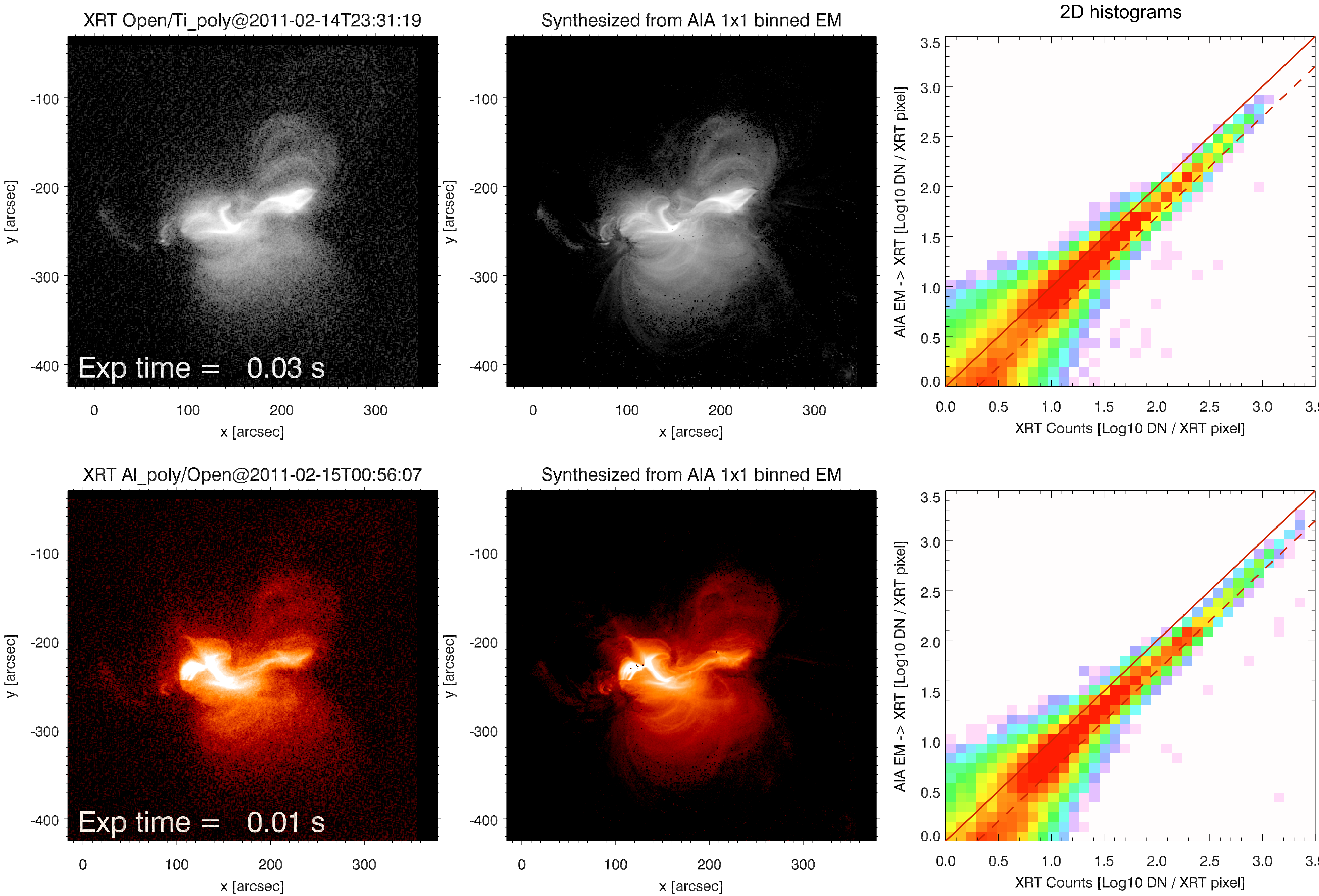

Also, see Su et al. (2018) for validation against RHESSI.

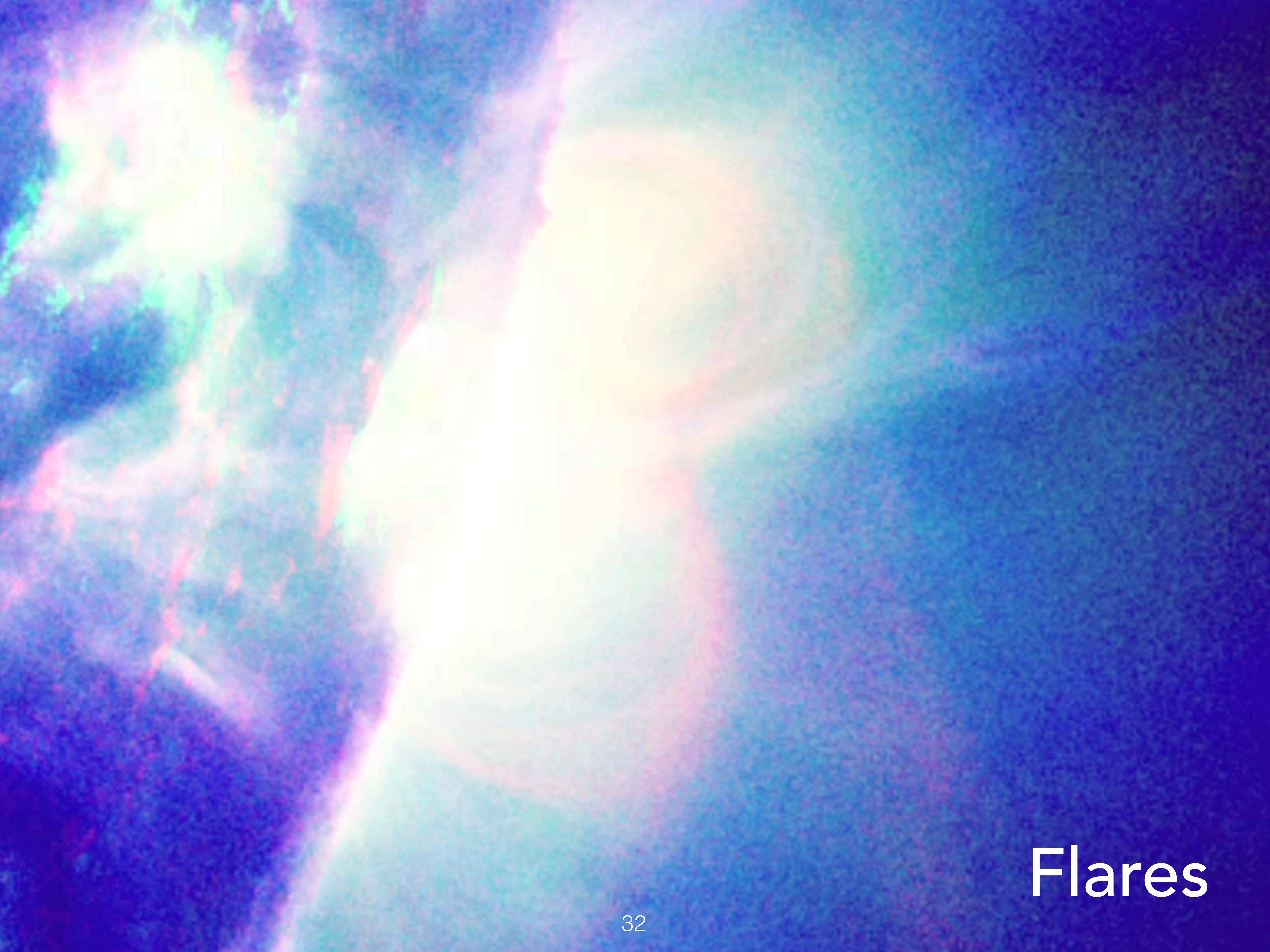

Flares

Application to a limb flare to track chromospheric evaporation

M7.7 limb flare

- Patsourakos, Vourlidas & Stenborg, 2013, *ApJ*, **764**, 125
- Wei Liu, Chen & Petrosian, 2013, *ApJ*, **767**, 168
- Rui Liu, 2013, *MNRAS*, **434**, 1309
- Krücker & Battaglia , 2014, *ApJ*, **780**, 107
- Sun, Cheng & Ding, 2014, *ApJ*, **786**, 73
- Krücker et al., 2015, *ApJ*, **802**, 19

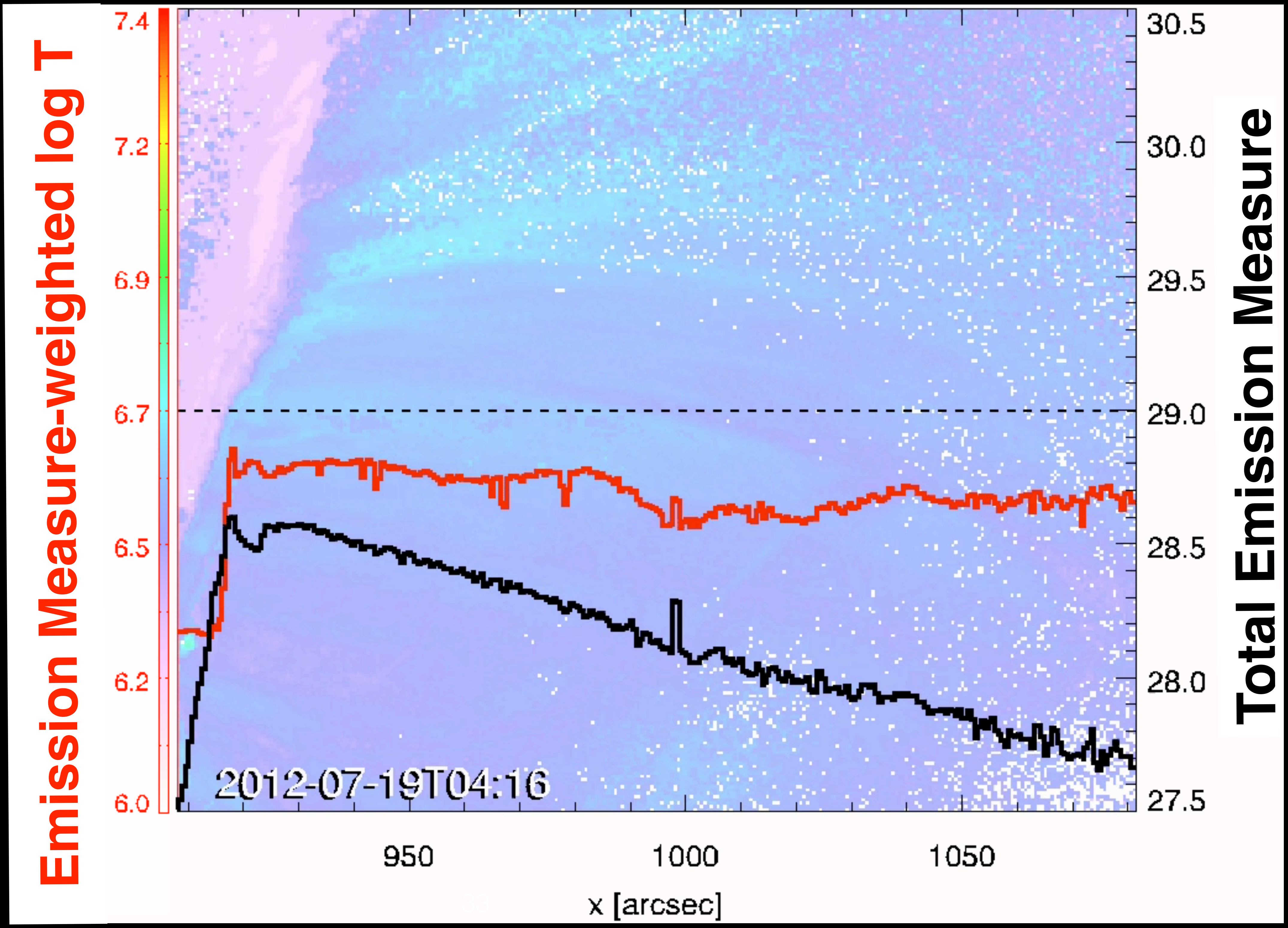

Application to a limb flare to track chromospheric evaporation

M7.7 limb flare

- Patsourakos, Vourlidas & Stenborg, 2013, *ApJ*, **764**, 125
- Wei Liu, Chen & Petrosian, 2013, *ApJ*, **767**, 168
- Rui Liu, 2013, *MNRAS*, **434**, 1309
- Krücker & Battaglia , 2014, *ApJ*, **780**, 107
- Sun, Cheng & Ding, 2014, *ApJ*, **786**, 73
- Krücker et al., 2015, *ApJ*, **802**, 19

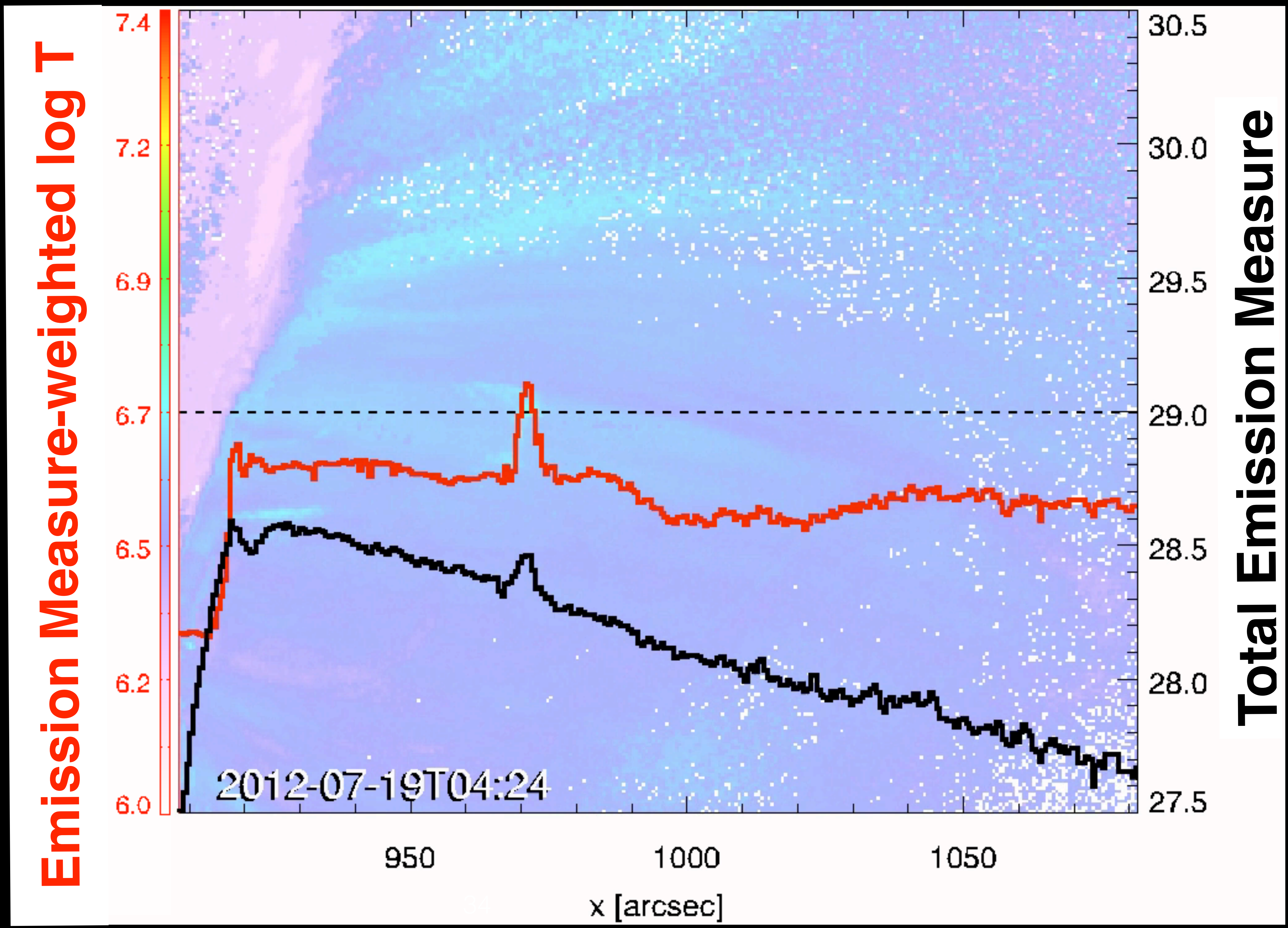

Application to a limb flare to track chromospheric evaporation

M7.7 limb flare

- Patsourakos, Vourlidas & Stenborg, 2013, *ApJ*, **764**, 125
- Wei Liu, Chen & Petrosian, 2013, *ApJ*, **767**, 168
- Rui Liu, 2013, *MNRAS*, **434**, 1309
- Krücker & Battaglia , 2014, *ApJ*, **780**, 107
- Sun, Cheng & Ding, 2014, *ApJ*, **786**, 73
- Krücker et al., 2015, *ApJ*, **802**, 19

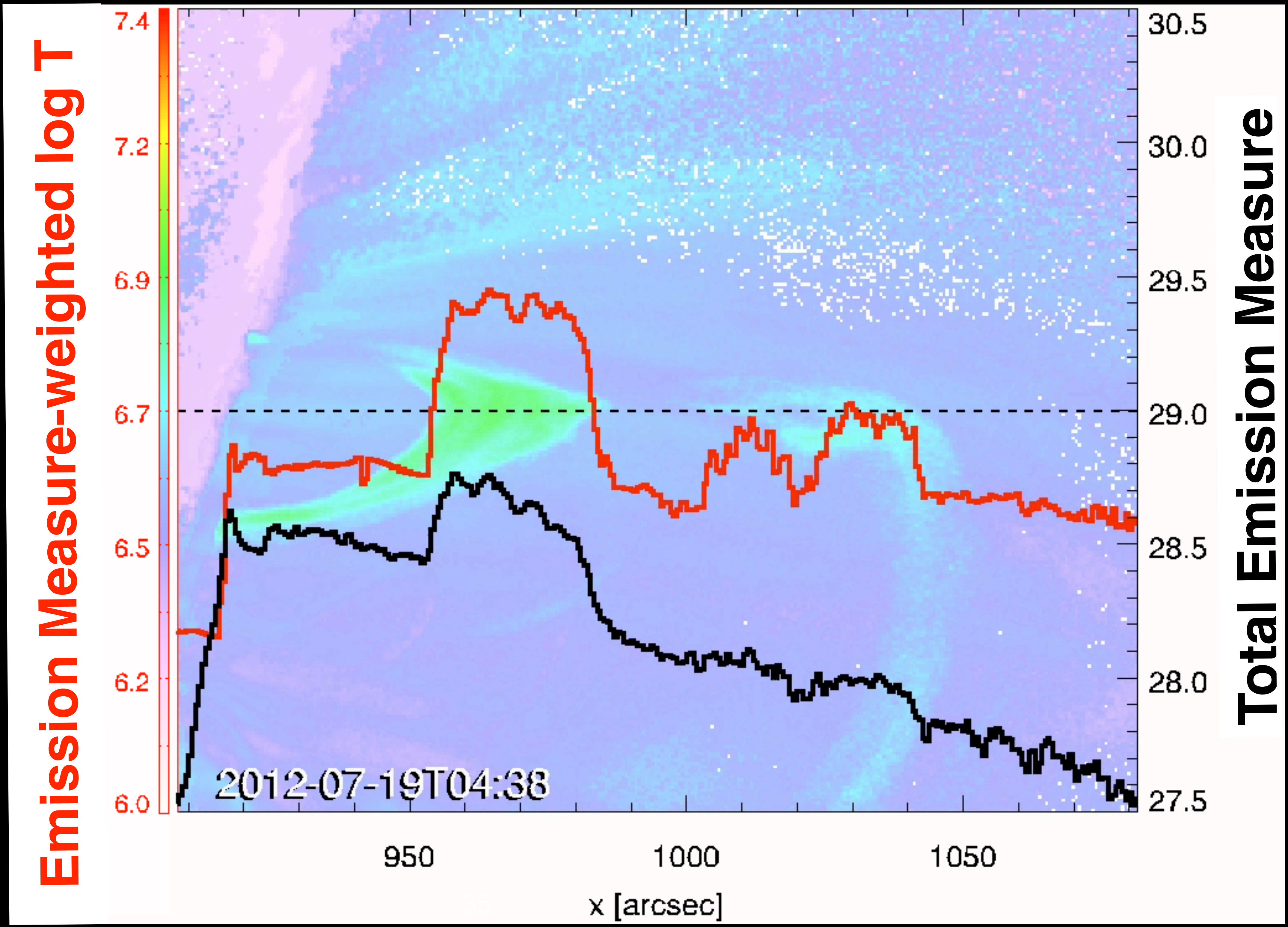

Application to a limb flare to track chromospheric evaporation

M7.7 limb flare

- Patsourakos, Vourlidas & Stenborg, 2013, *ApJ*, **764**, 125
- Wei Liu, Chen & Petrosian, 2013, *ApJ*, **767**, 168
- Rui Liu, 2013, *MNRAS*, **434**, 1309
- Krücker & Battaglia , 2014, *ApJ*, **780**, 107
- Sun, Cheng & Ding, 2014, *ApJ*, **786**, 73
- Krücker et al., 2015, *ApJ*, **802**, 19

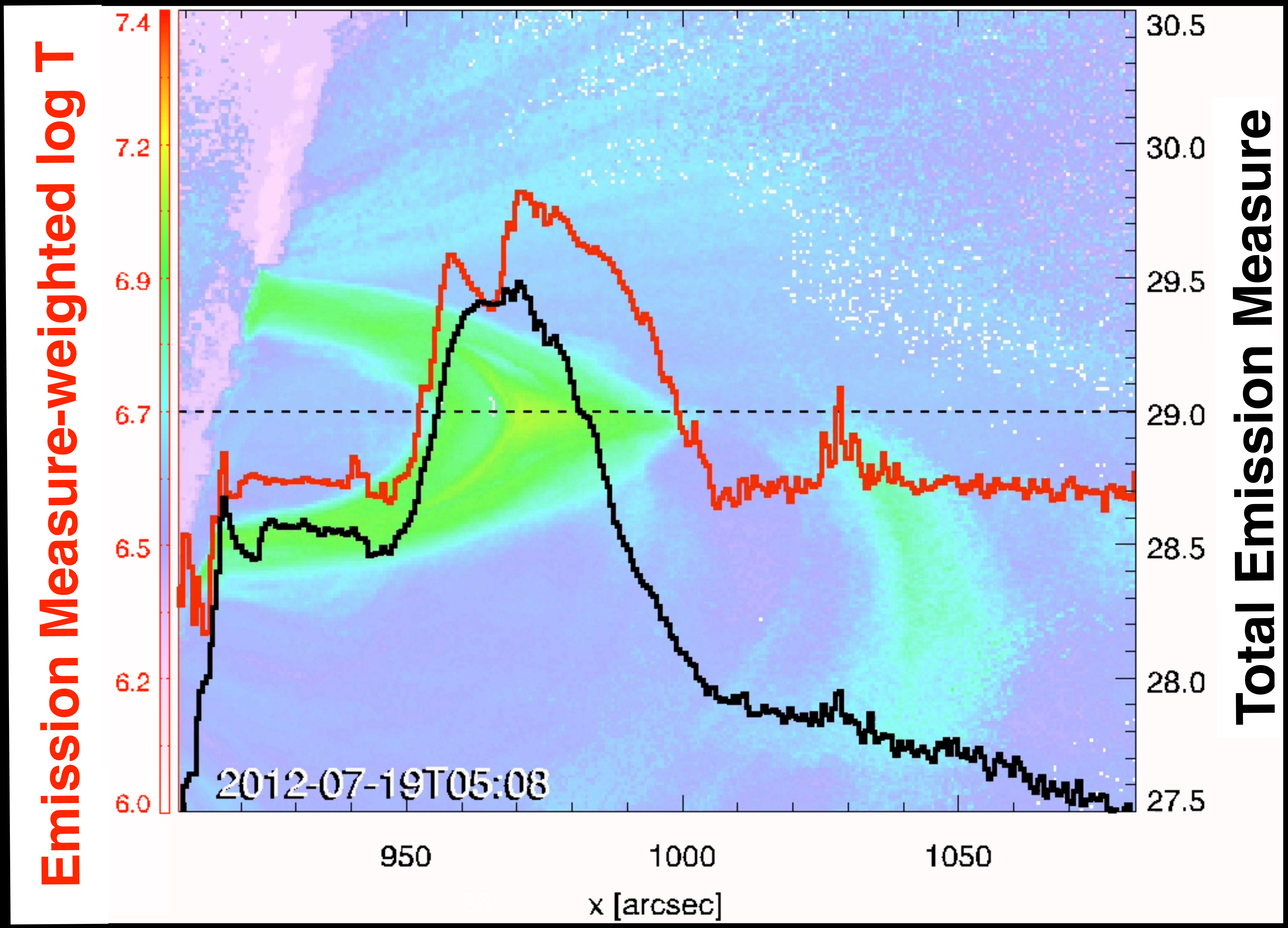

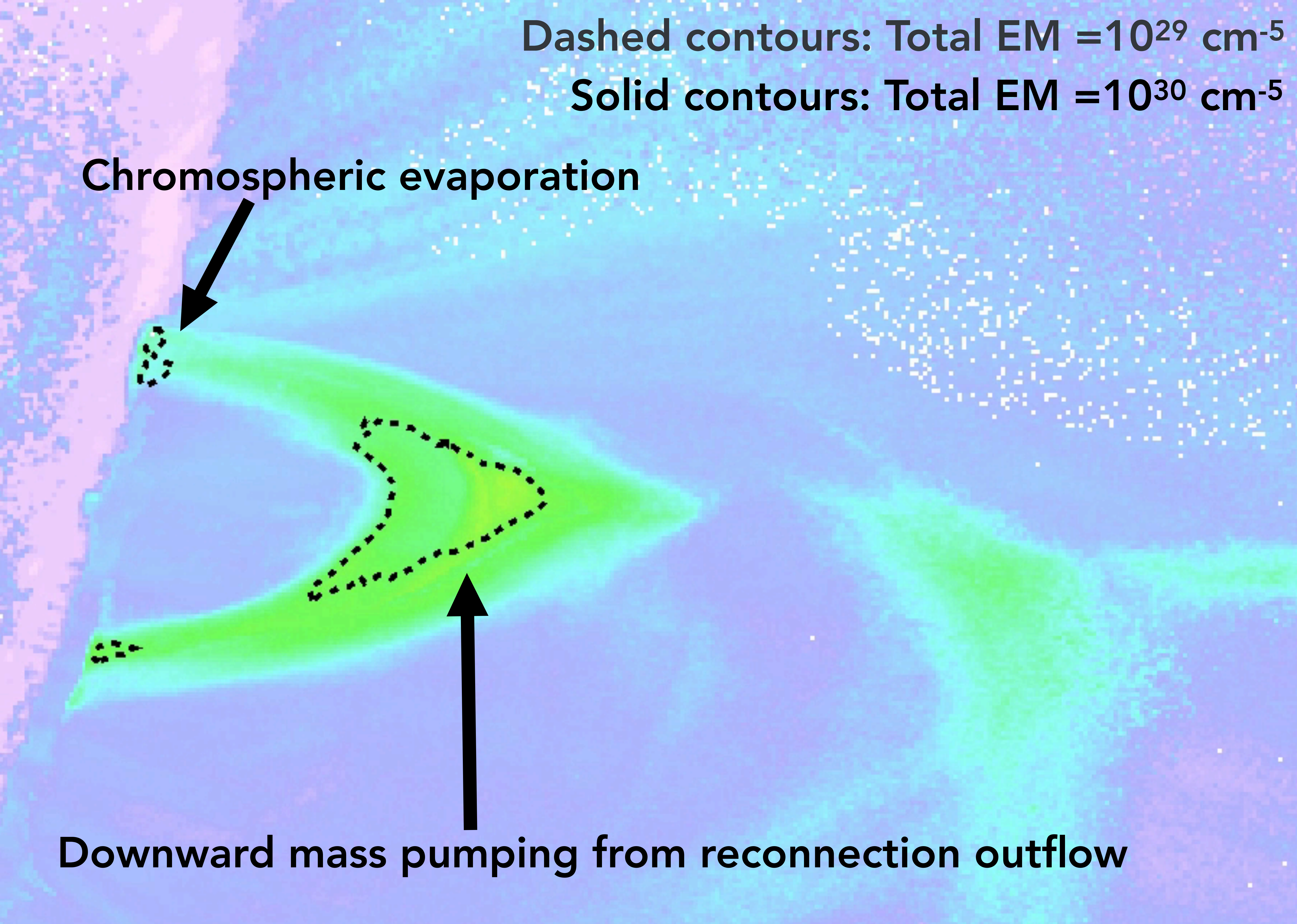
Dashed contours: Total EM =10^29 cm^-5
Solid contours: Total EM =10^30 cm^-5
Chromospheric evaporation
Downward mass pumping from reconnection outflow

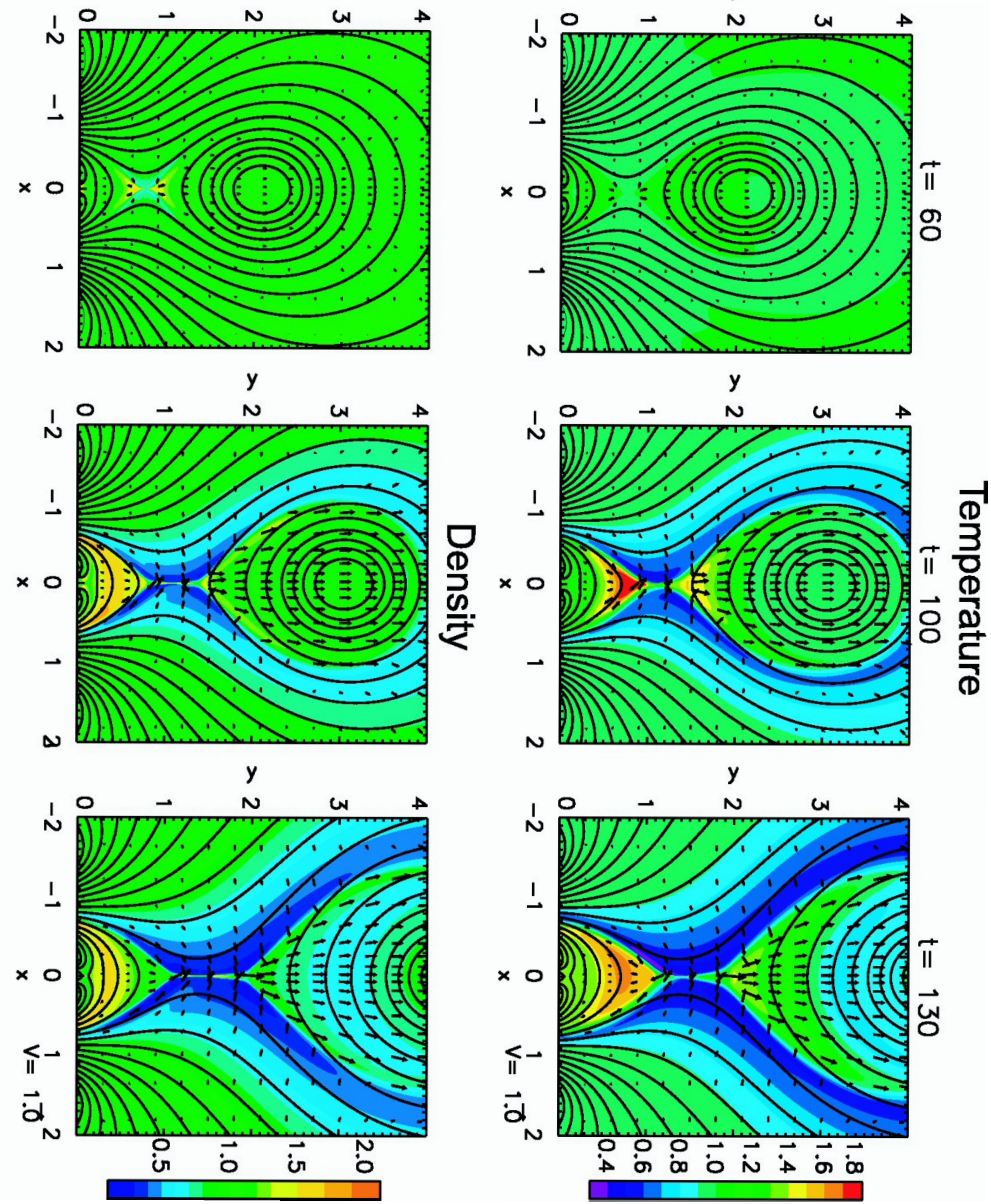

Shiota et al. (2005, ApJ, **634**, 663):

- 2.5D MHD simulation of of the eruption of a pre-existing flux rope triggered by flux emergence.
- Similar scenario as modeled by Chen & Shibata (2000, ApJ, **545**, 524) but with field-aligned thermal conduction.
- Both temperature and density are initially uniform (dimensionless value of unity).

Influence of efficiency of thermal conduction / system size

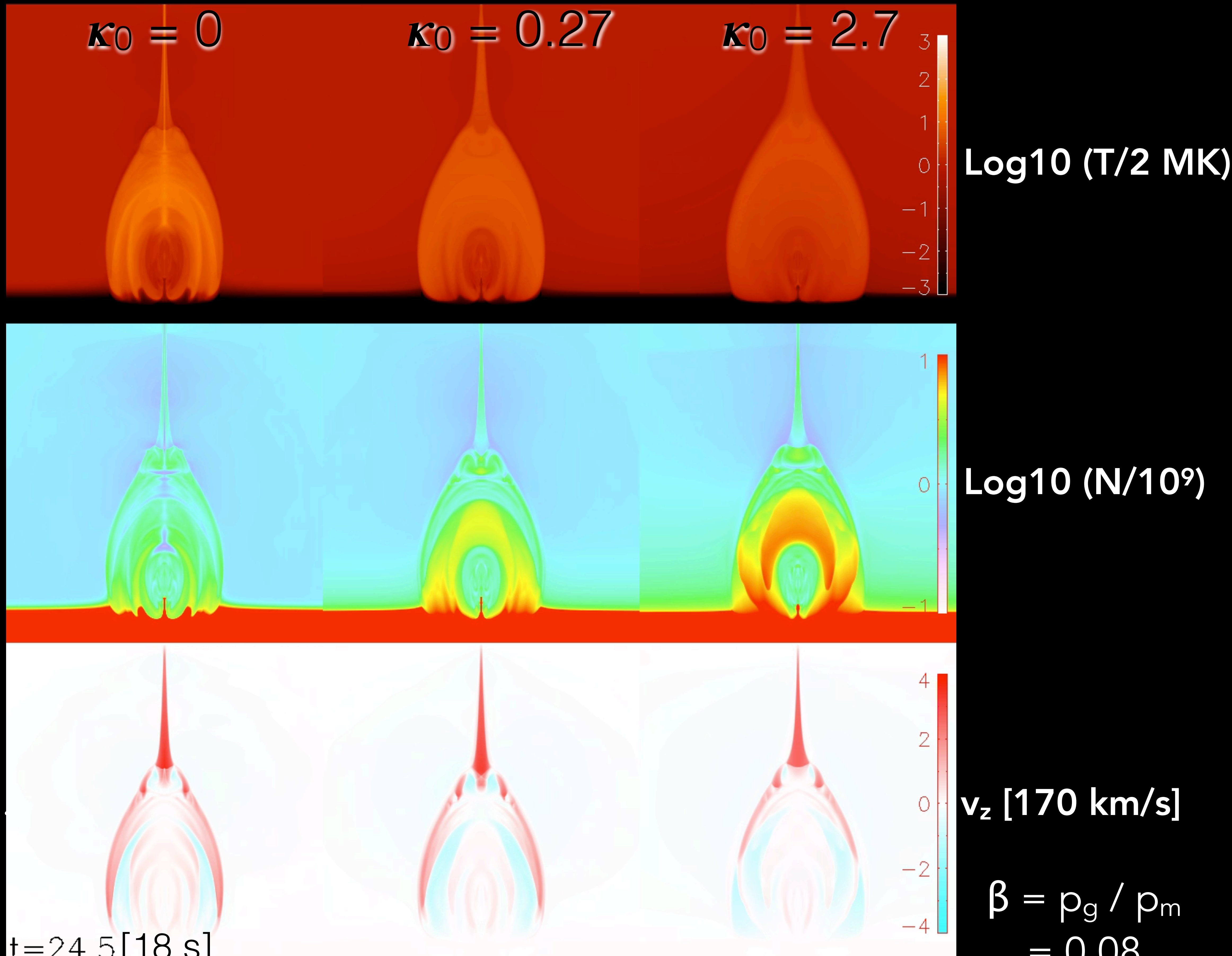

Extension of study by Takasao et al. (ApJ, 2015, **805**, 135)

$\beta = p_g / p_m = 0.08$

Influence of efficiency of thermal conduction / system size

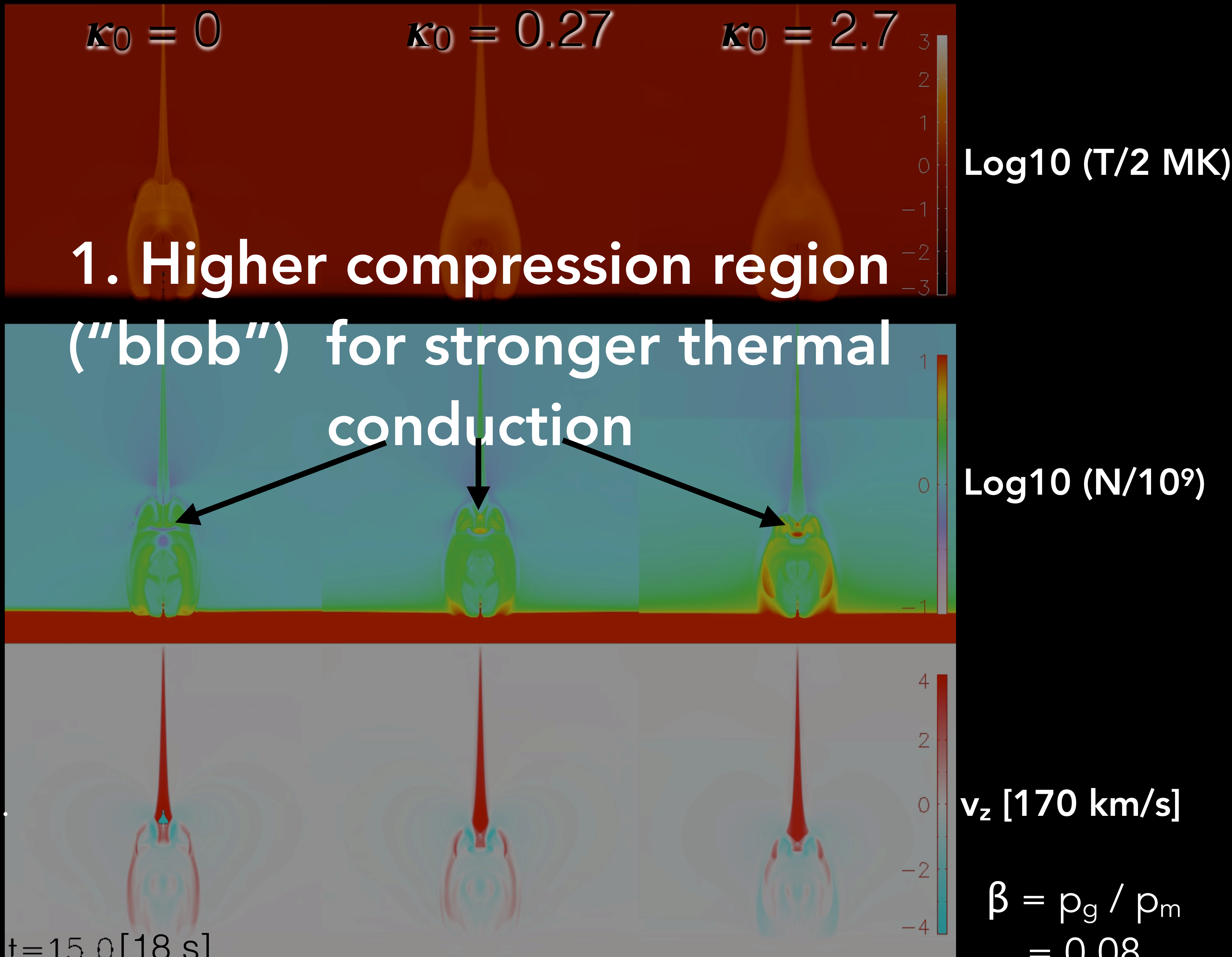

Extension of study by Takasao et al. (ApJ, 2015, **805**, 135)

$\beta = p_g / p_m = 0.08$

Influence of efficiency of thermal conduction / system size

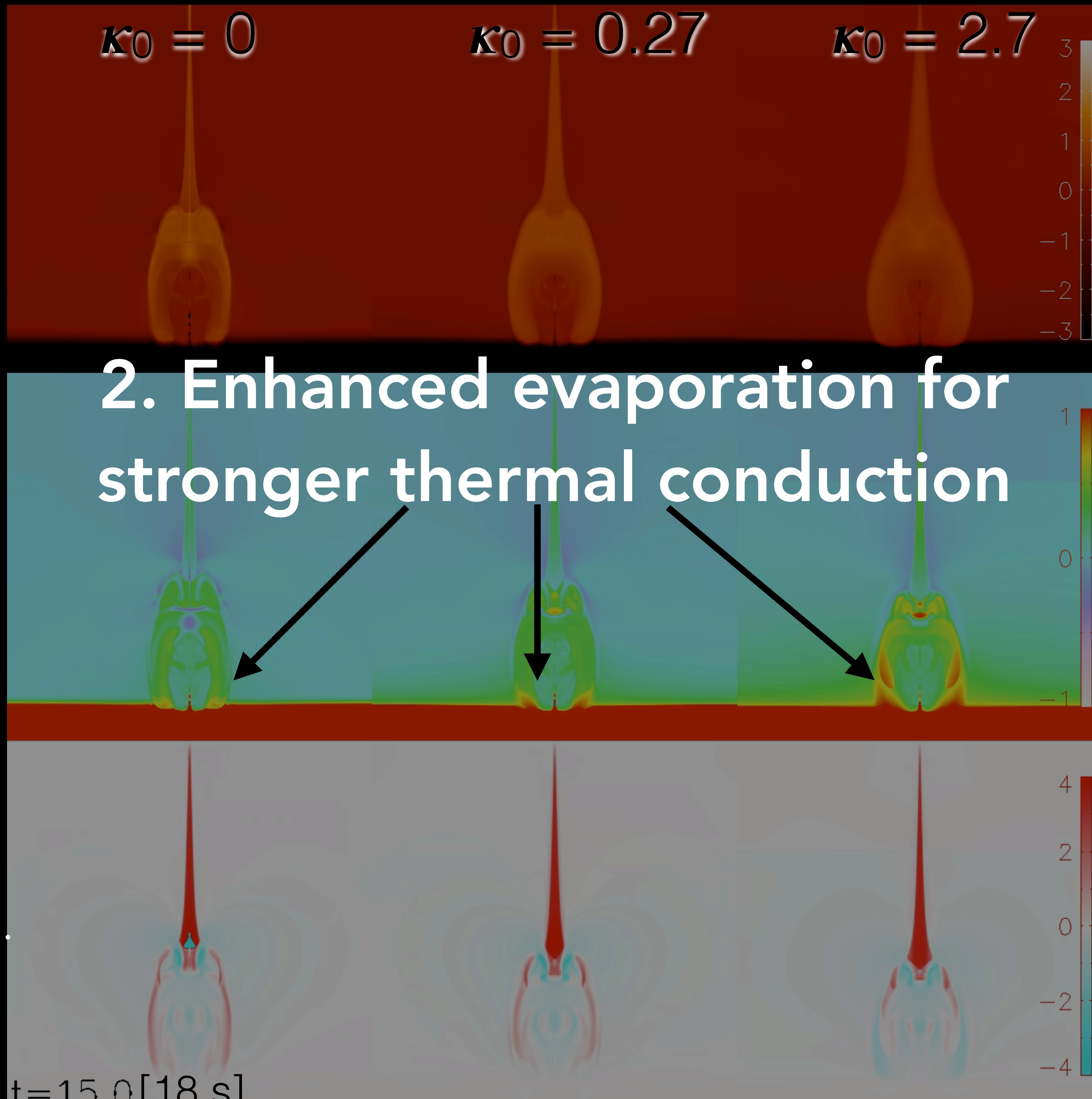

Log10 (T/2 MK)

Log10 (N/10⁹)

v_z [170 km/s]

$\beta = p_g / p_m = 0.08$

Extension of study by Takasao et al. (ApJ, 2015, **805**, 135)

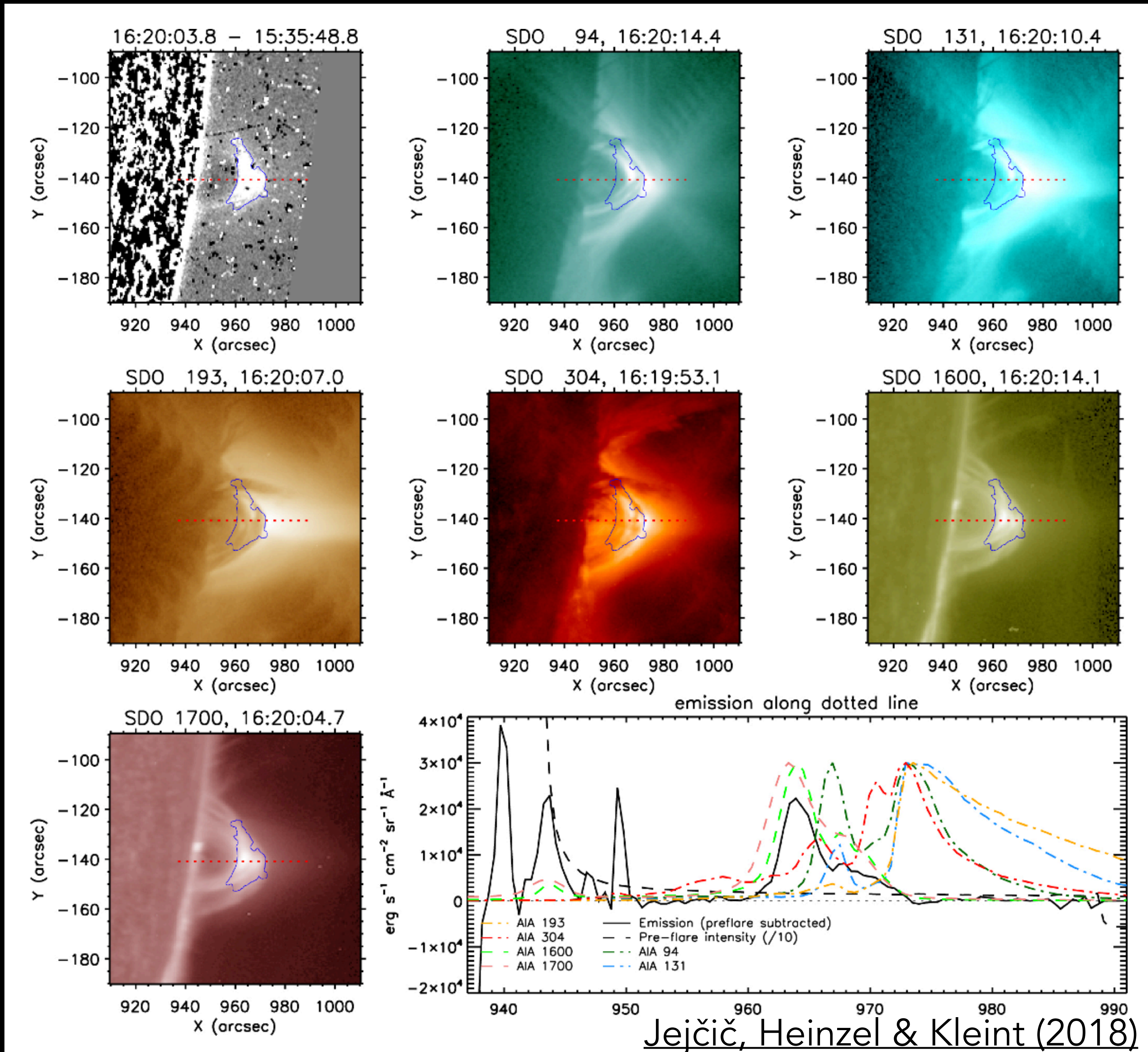

Shibayama et al. (2013) ...
Estimated energies of Kepler superflares assuming black-body radiation @ 10,000 K plasma at the base of flare loops (ribbons).

Jejčič, Heinzel & Kleint (2018): SDO Observations of X8.2 limb flare-loop emission detected in SDO/HMI (see also Heinzel et al 2017).

Heinzel & Shibata (2018):
" This new scenario for interpreting superflare emission suggests that the observed WL flux is due to a mixture of the ribbon and loop radiation and can be even loop-dominated during the gradual phase of superflares."

NASA Heliophysics Grand Challenges Research (HGCR): Physics and Diagnostics of the Drivers of Solar Eruptions

Cheung, Rempel et al. (Nature Astronomy 2019)






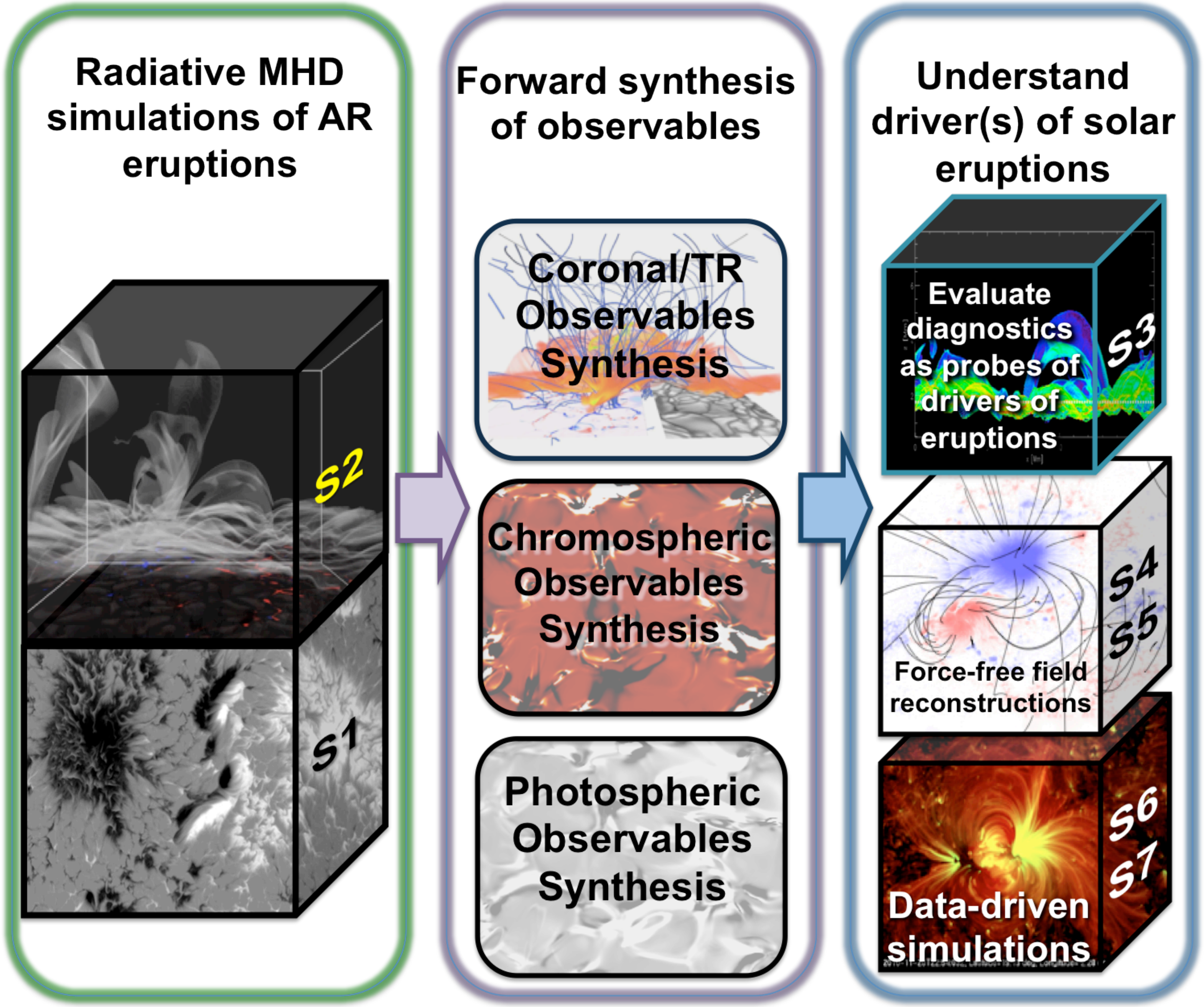








A collaboration between LMSAL (PI: Cheung), NCAR, BAERI, SAO & U Oslo, supported by NASA Grant NNX14AI14G

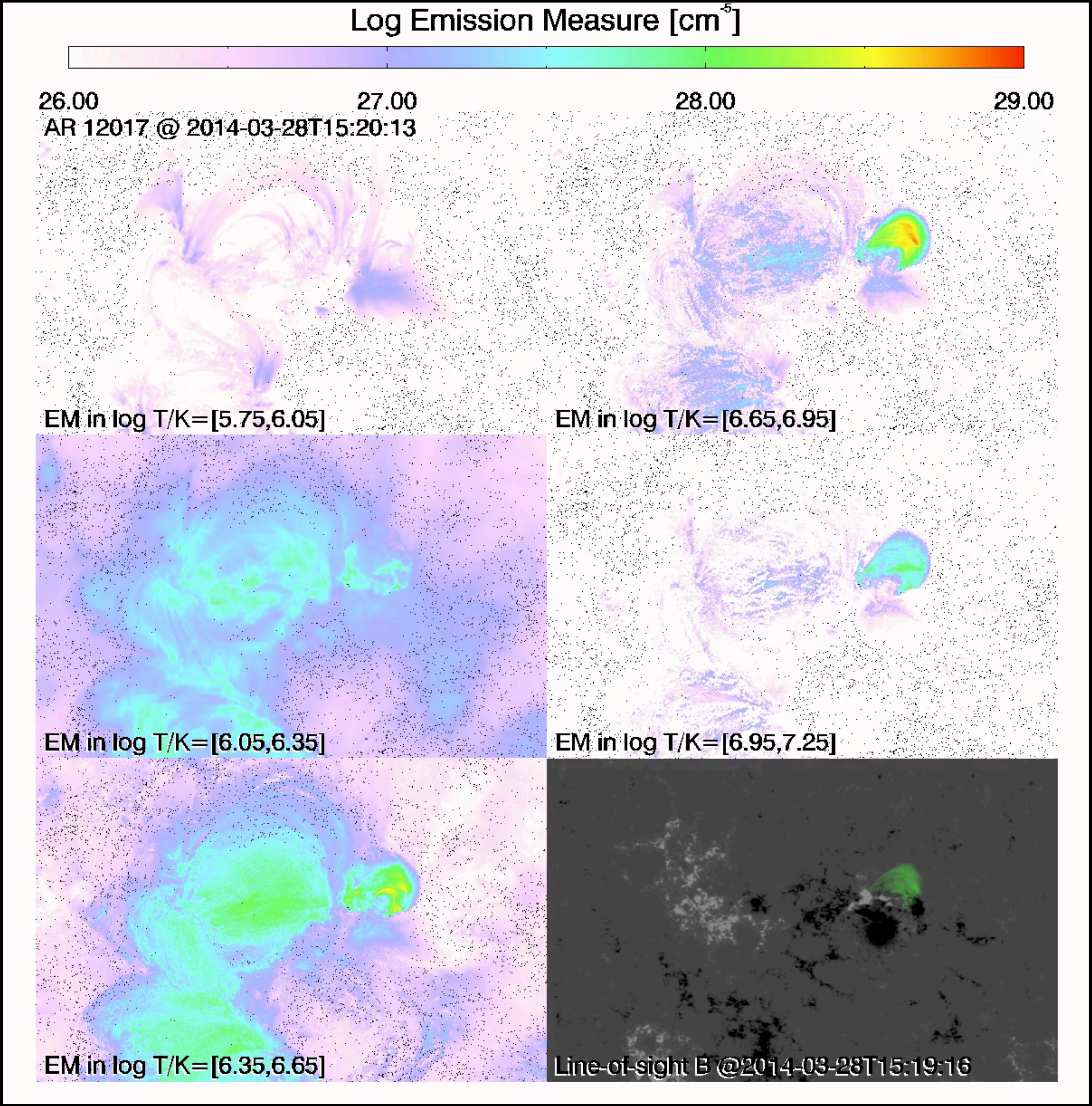

NOAA AR 12017:

one X-class ("Best Observed X-flare"), 3 M-class, and about two dozen C-class flares

Sunquake: Judge et al. (2014)

Filament Eruption before X-flare: Kleint et al. (2015)

IRIS Fe XXI FUV spectra: Young et al. (2015)

Chromospheric Evaporation: Li et al. (2015)

Sunspots Simulation with MURaM

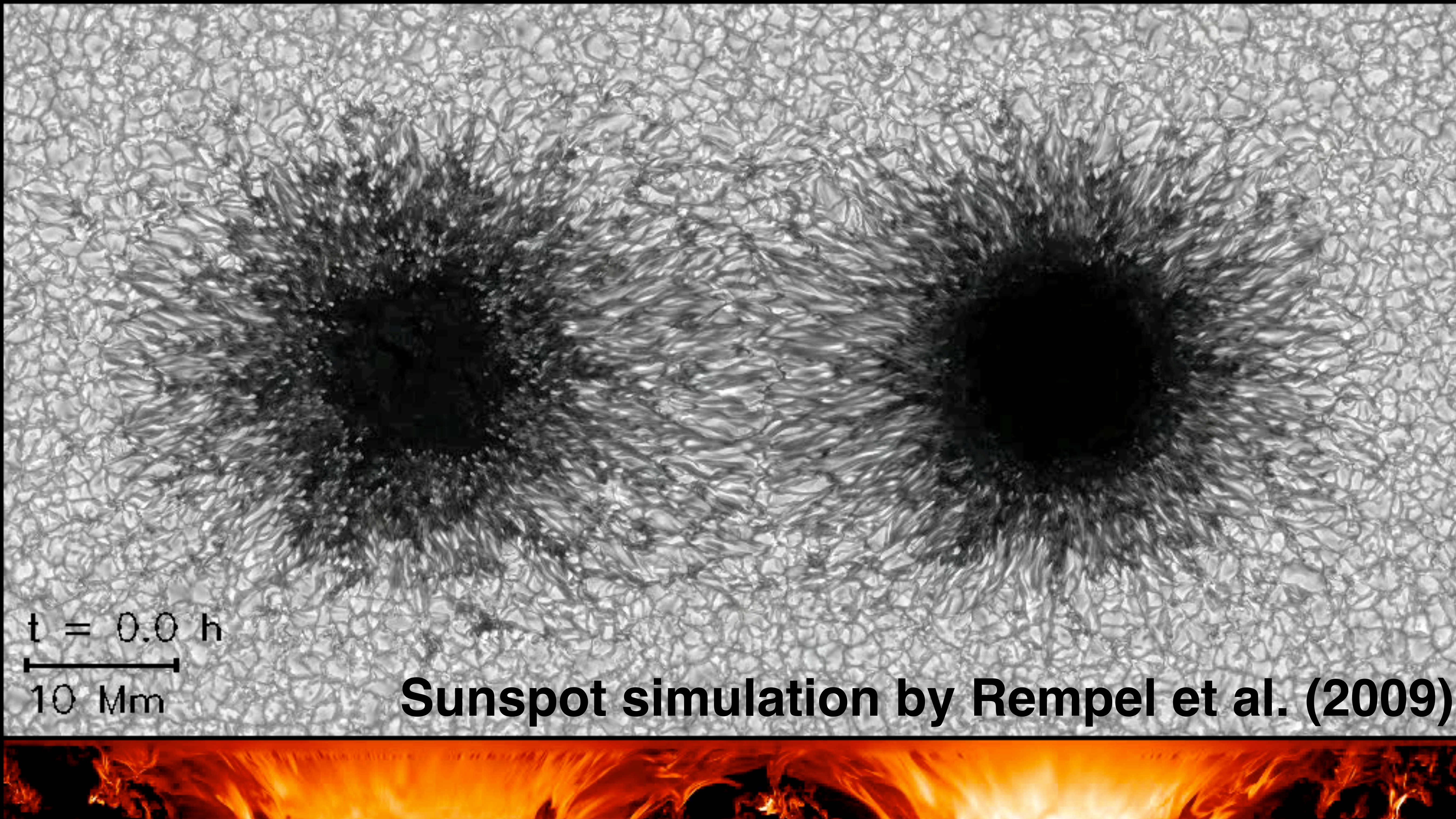

Top: Emergent gray intensity. Bottom: Vertical slice of |B|

Synthetic GOES X-ray Light Curves

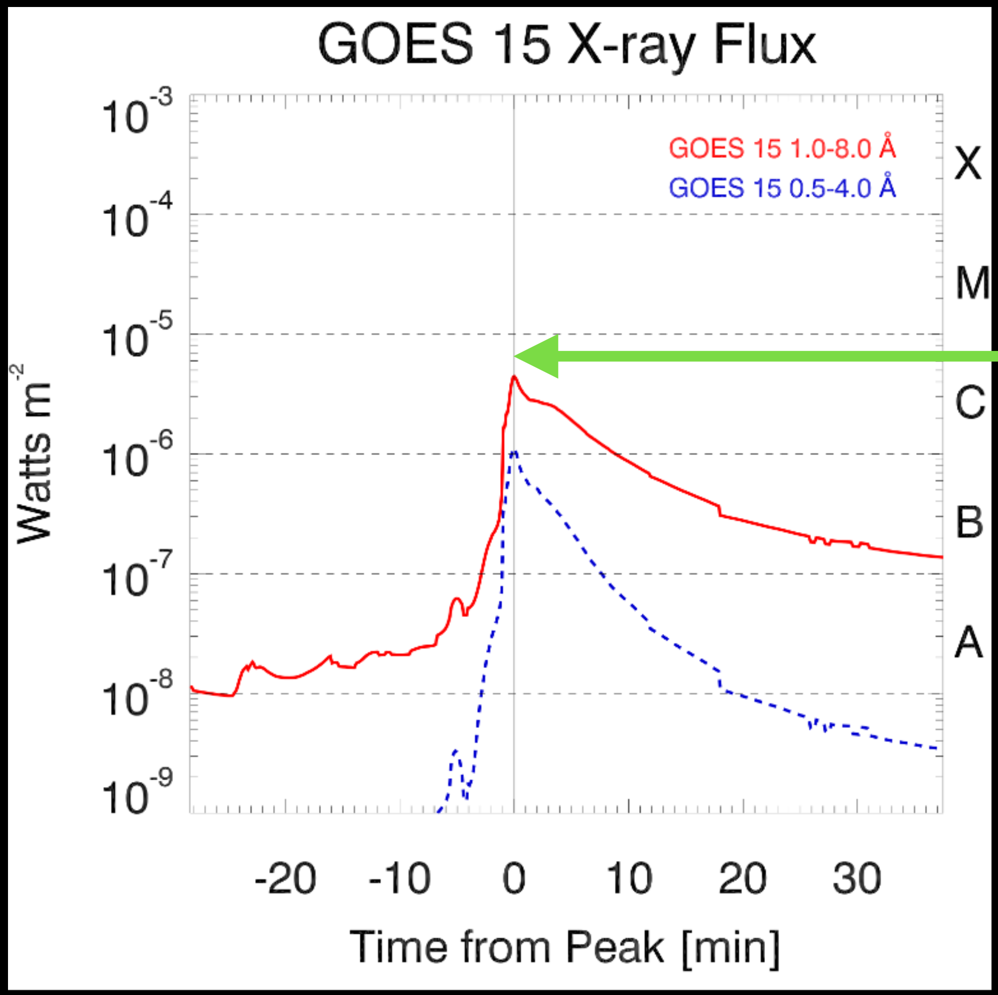

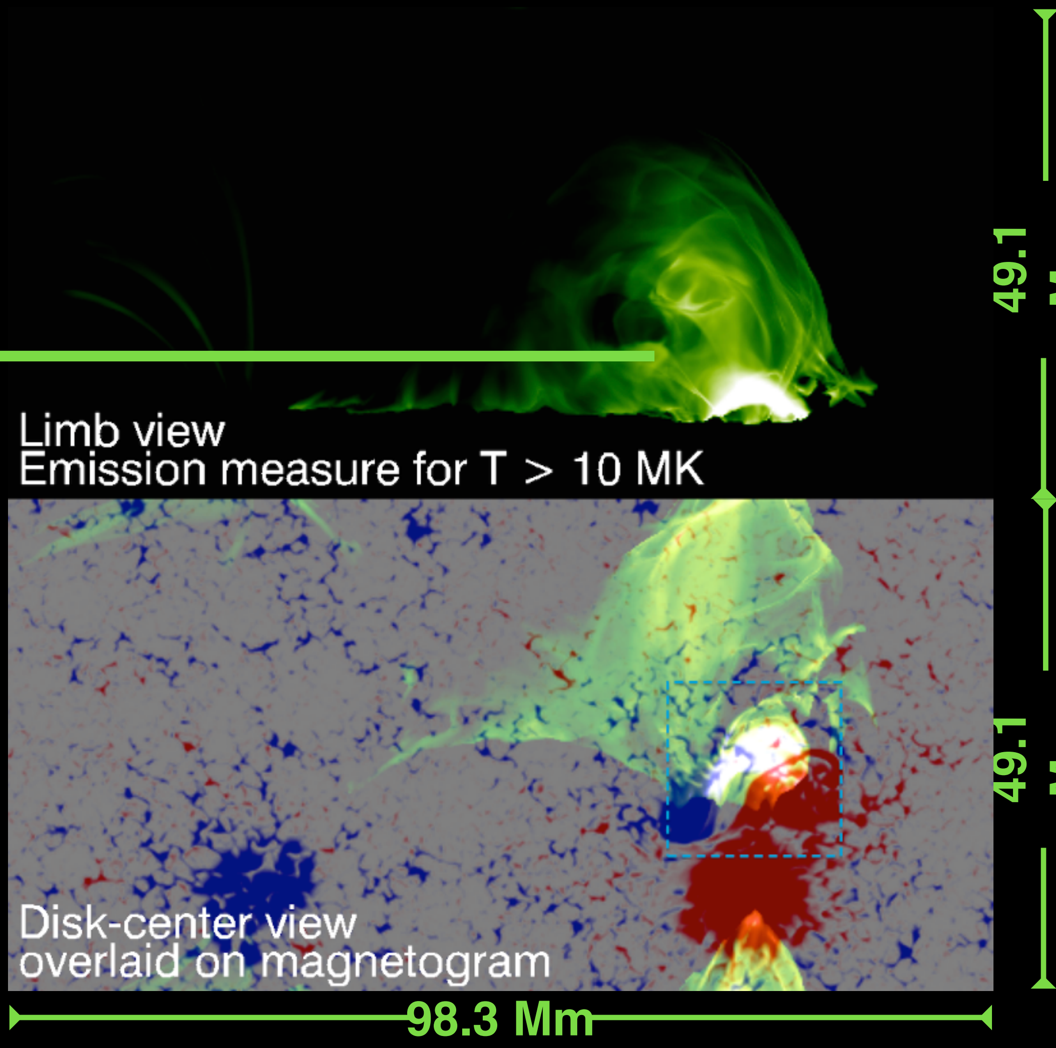

C4 flare if measured by detectors on GOES 15. The free magnetic energy (actual minus potential field) dropped by ~5x10^{30} erg (~10%) over 5 minutes.

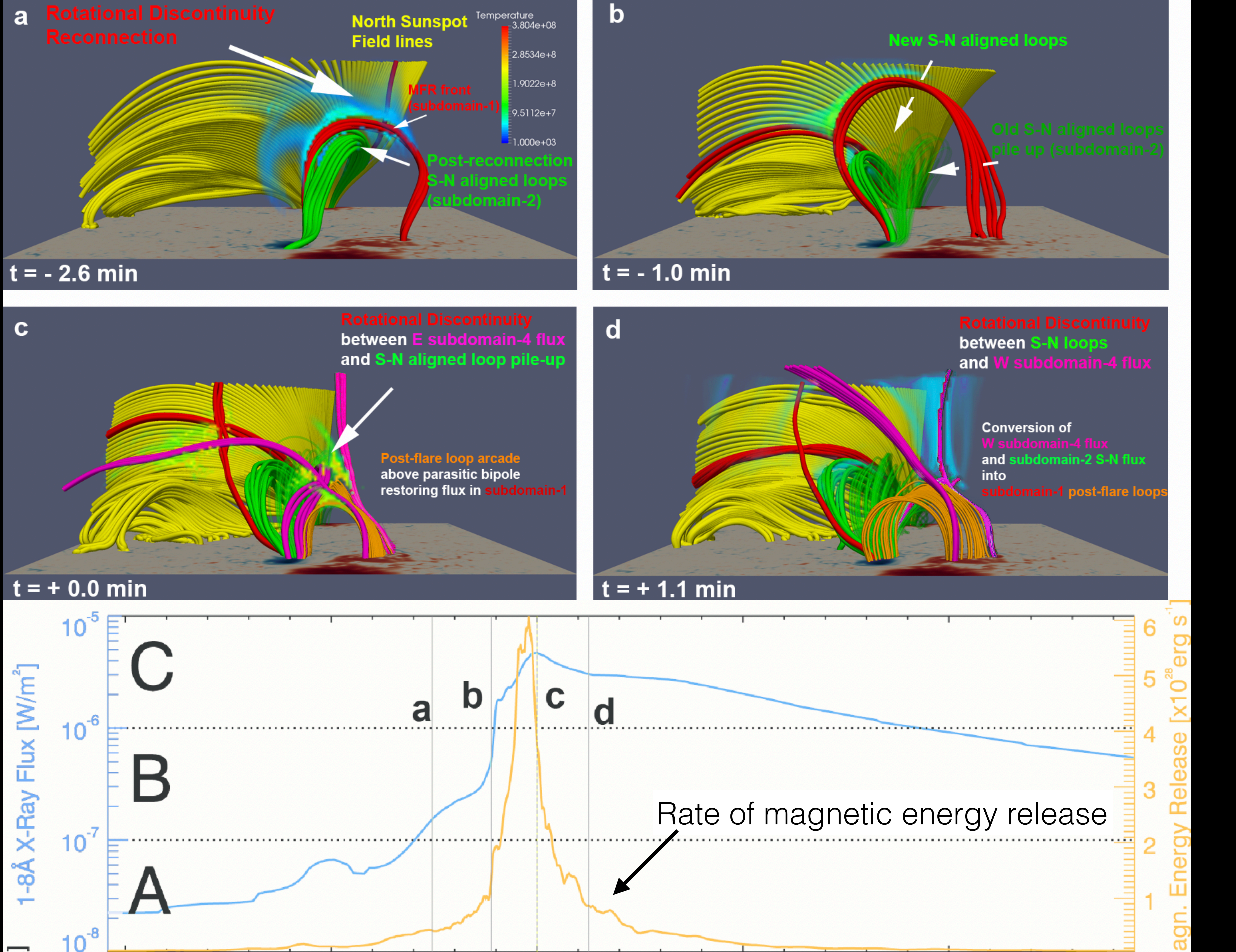

a
Rotational Discontinuity Reconnection
North Sunspot Field lines
Temperature
3.804e+08
2.8534e+8
1.9022e+8
9.5112e+7
1.000e+03
MFR front (subdomain-1)
Post-reconnection S-N aligned loops (subdomain-2)
t = - 2.6 min
b
New S-N aligned loops
Old S-N aligned loops pile up (subdomain-2)
t = - 1.0 min
c
Rotational Discontinuity between E subdomain-4 flux and S-N aligned loop pile-up
Post-flare loop arcade above parasitic bipole restoring flux in subdomain-1
t = + 0.0 min
d
Rotational Discontinuity between S-N loops and W subdomain-4 flux
Conversion of W subdomain-4 flux and subdomain-2 S-N flux into subdomain-1 post-flare loops
t = + 1.1 min
1-8Å X-Ray Flux [W/m²]
Magn. Energy Release [x10²⁸ erg s⁻¹]
C
B
A
a
b
c
d
Rate of magnetic energy release

Synthetic SDO/AIA EUV Images

Top down view

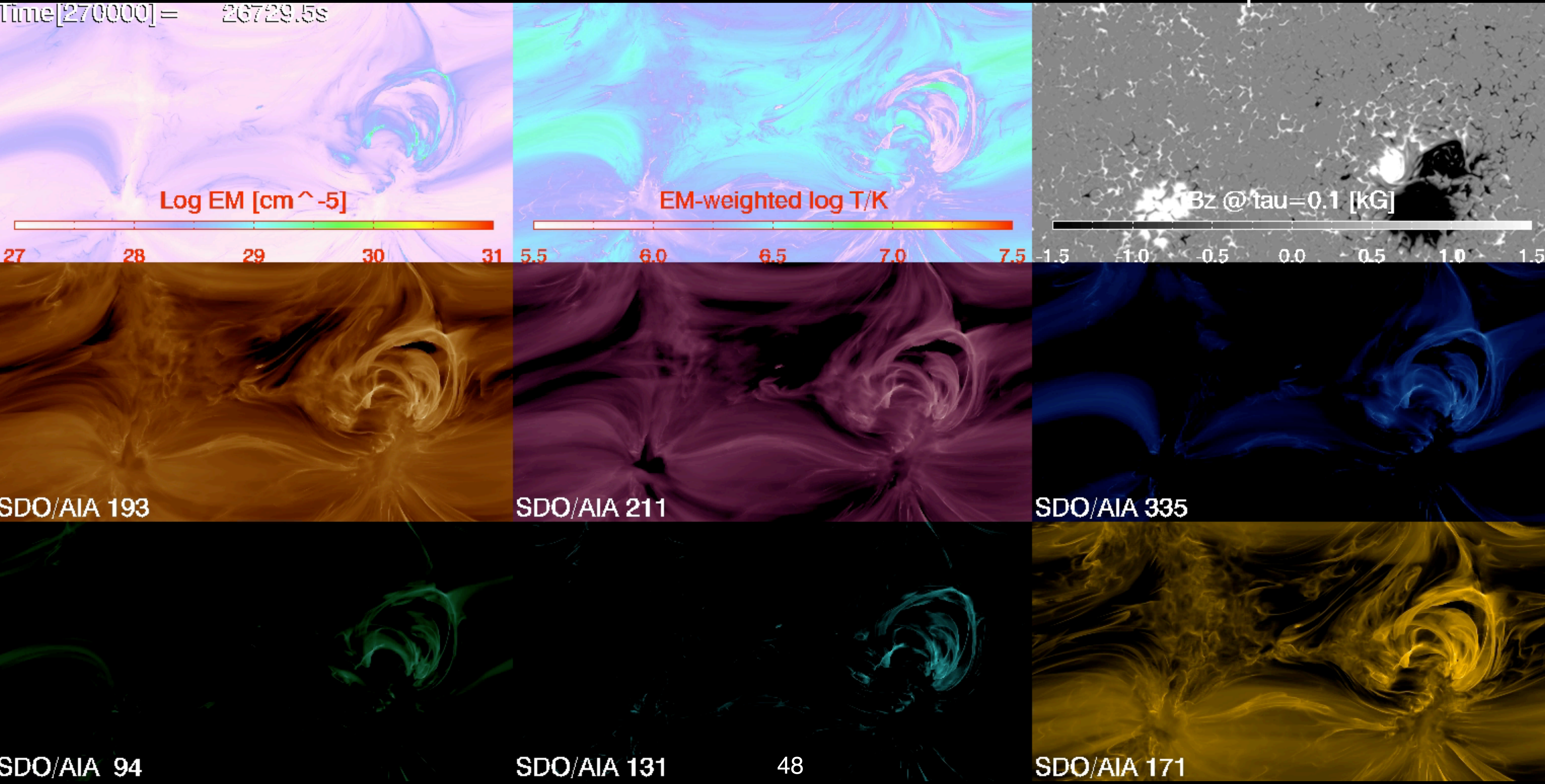

Simulation available at https://purl.stanford.edu/dv883vb9686

Synthetic Doppler Maps from Optically Thin Radiation

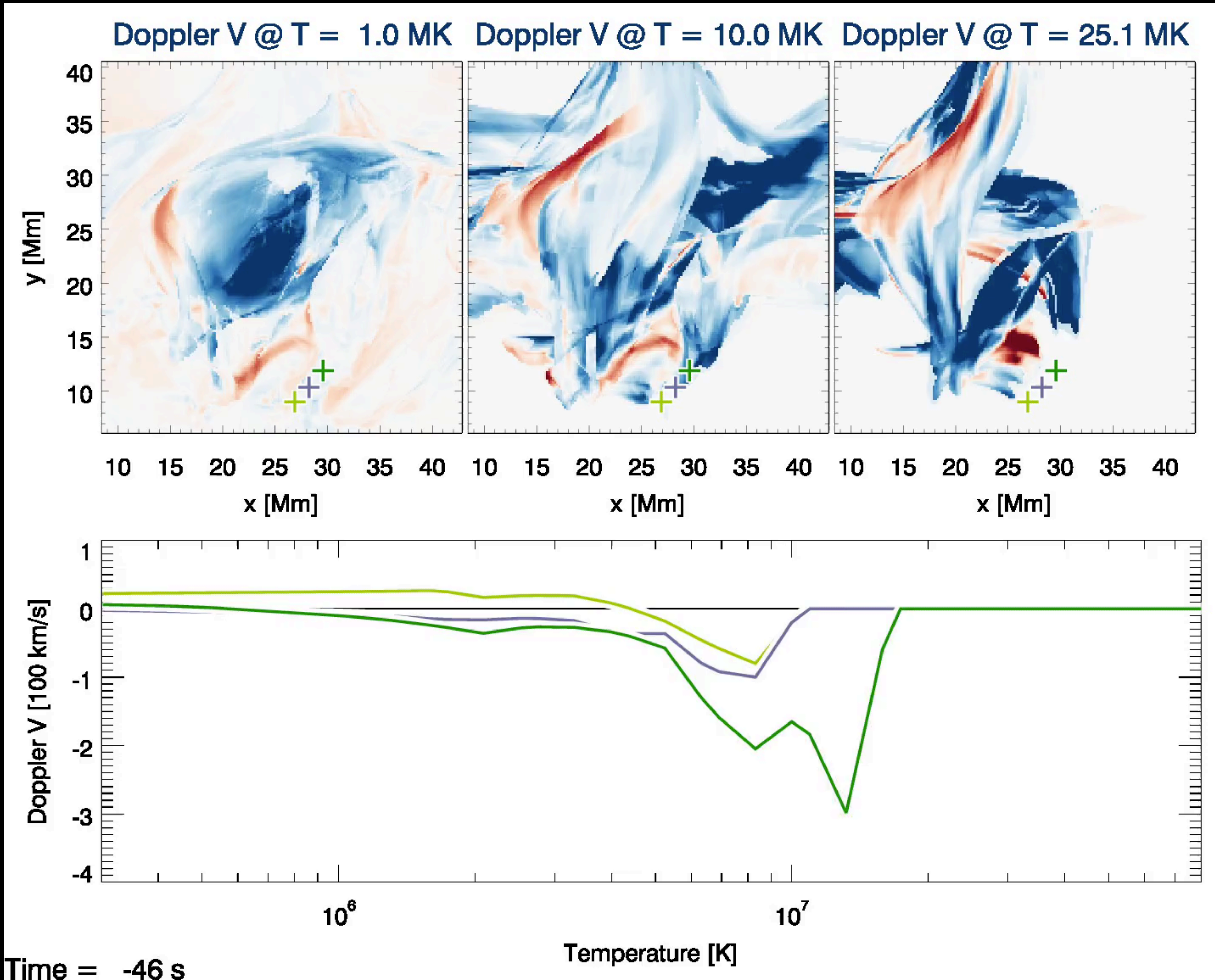

Using using thermal bremsstrahlung, the model yields power law-like shapes for the X-ray spectrum.

The multi-thermal nature of the magnetic structure gives rise to the apparent non-thermal behavior.

Above-the-loop-top harder X-ray sources (> 25 keV) are located above softer loop sources.

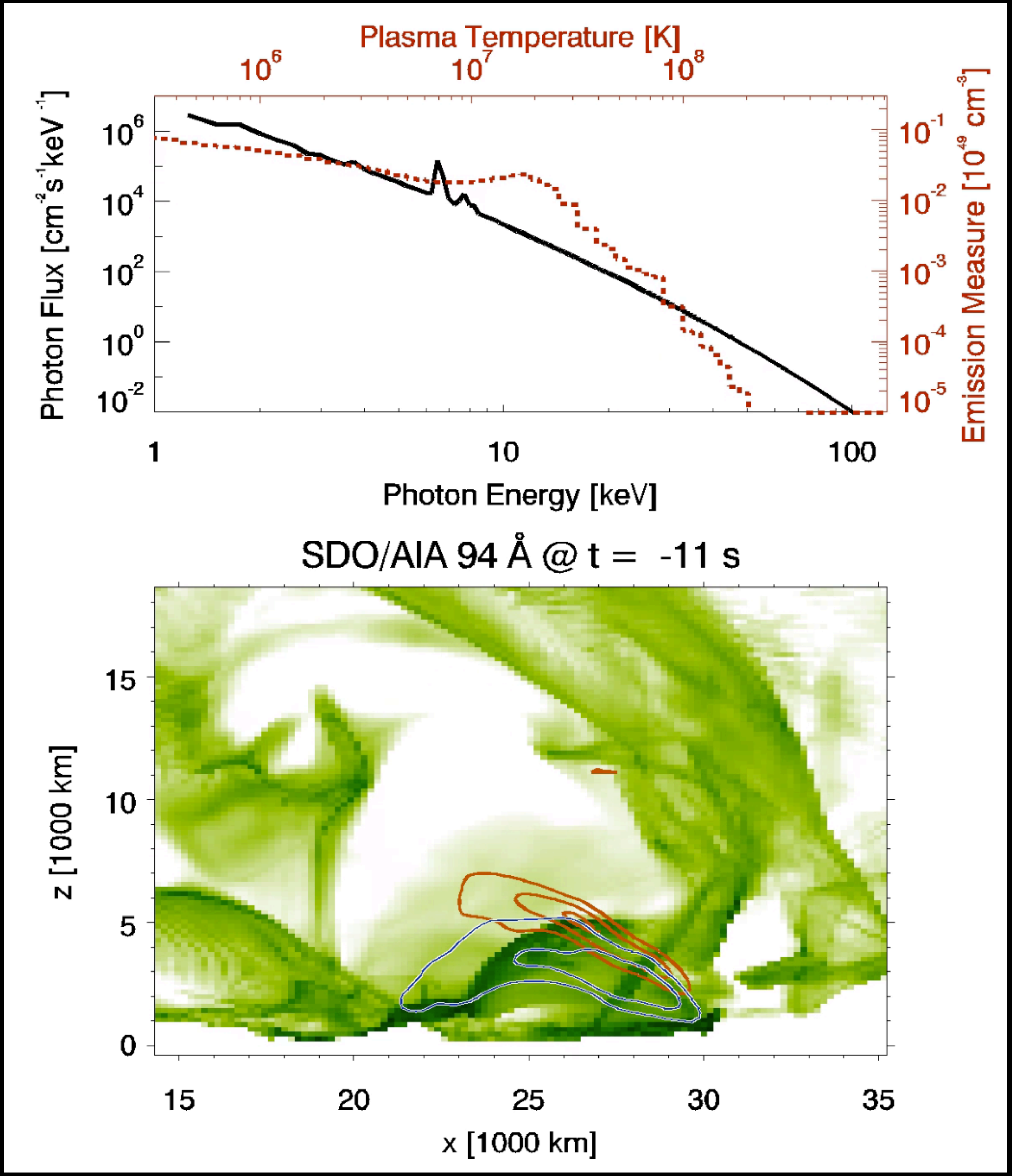

Hard x-rays ≥ 25 keV **6 ≤ Soft x-rays ≤ 12 keV**

Using using thermal bremsstrahlung, the model yields power law-like shapes for the X-ray spectrum.

The multi-thermal nature of the magnetic structure gives rise to the apparent non-thermal behavior.

Above-the-loop-top harder X-ray sources (> 25 keV) are located above softer loop sources.

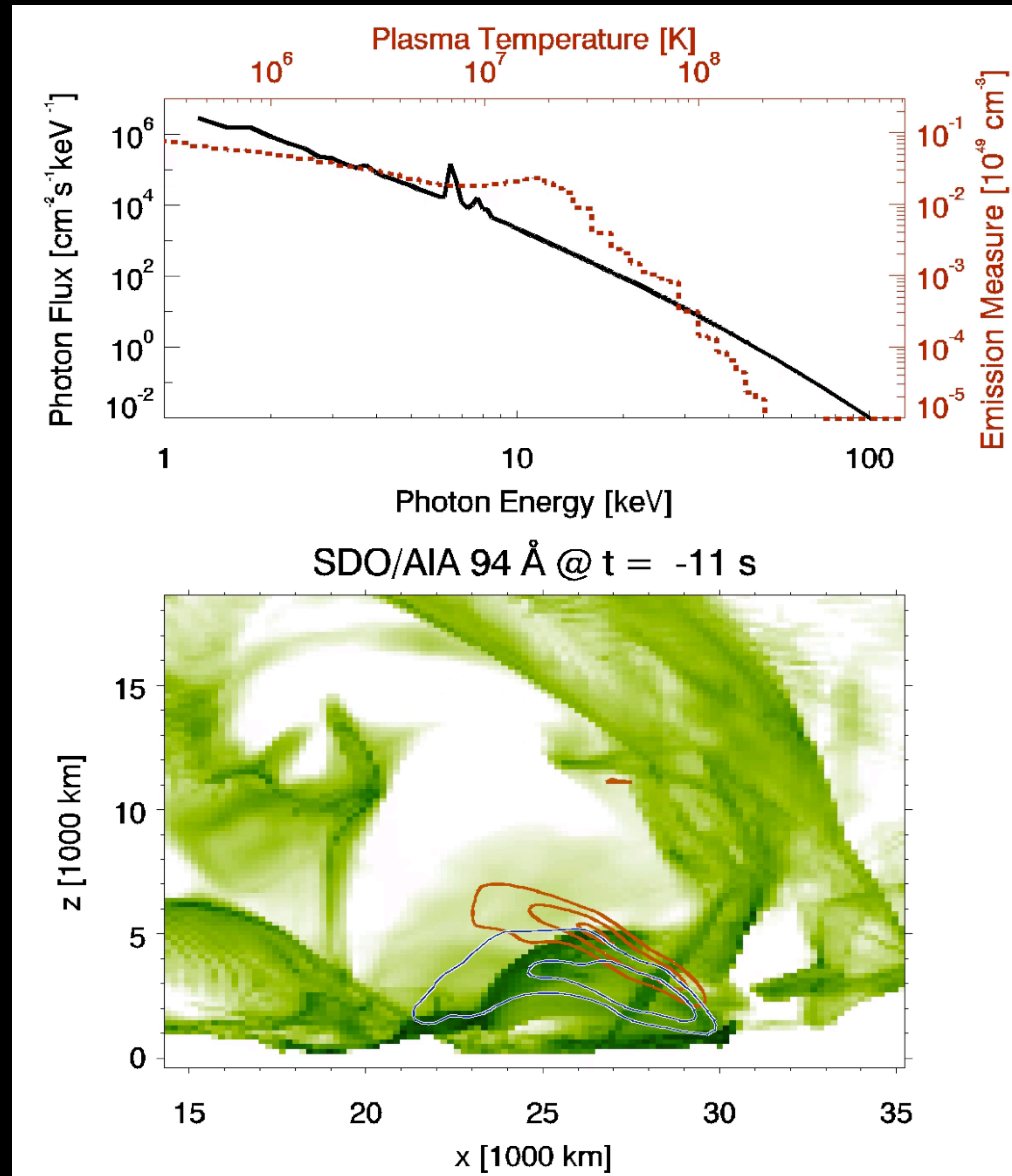

Hard x-rays ≥ 25 keV **6 ≤ Soft x-rays ≤ 12 keV**

Emergence into the Solar Atmosphere

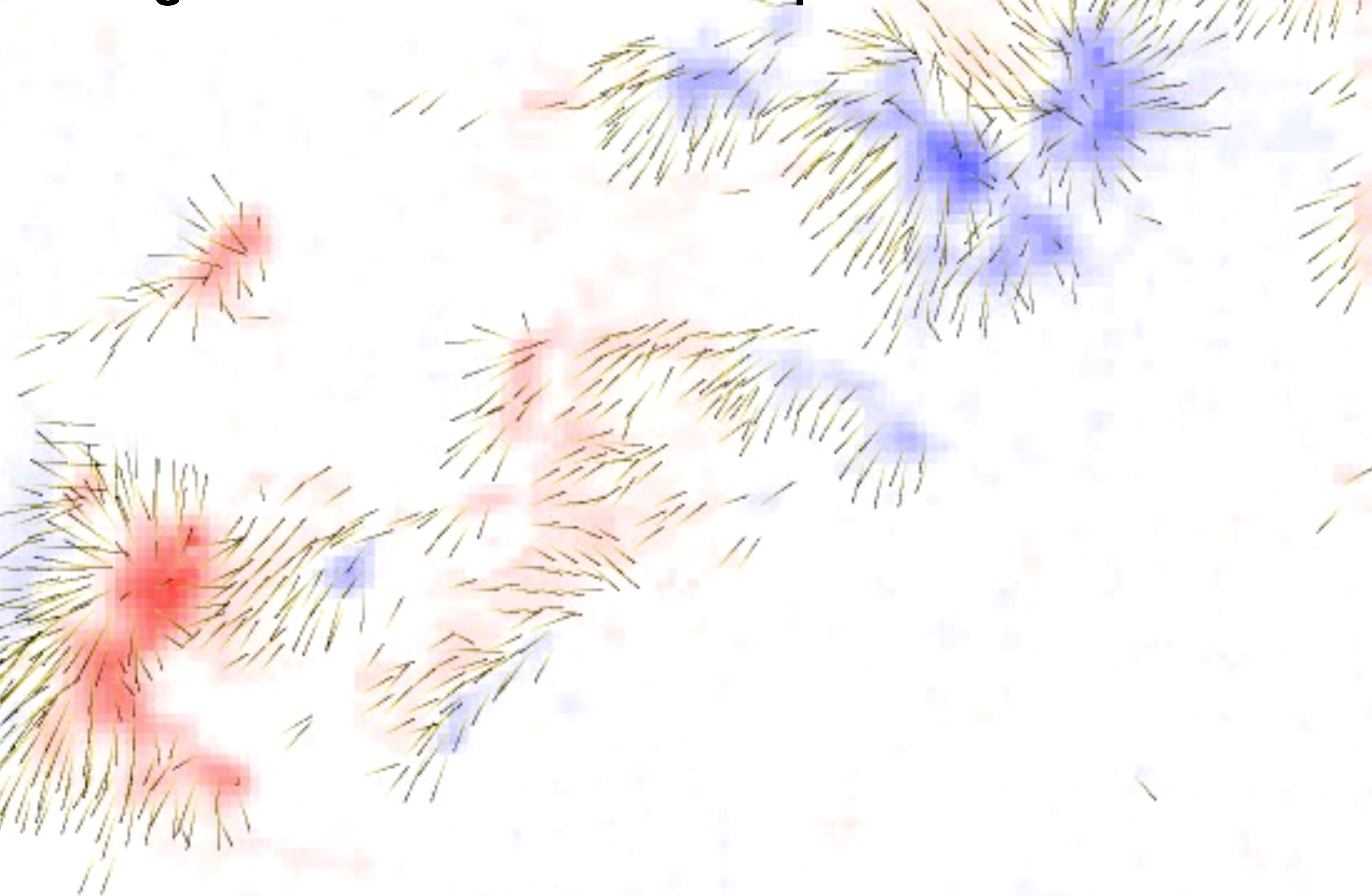

Credit: SDO/HMI (visualization by Keiji Hayashi)

"Magnetograms" from a Magnetofriction* simulation

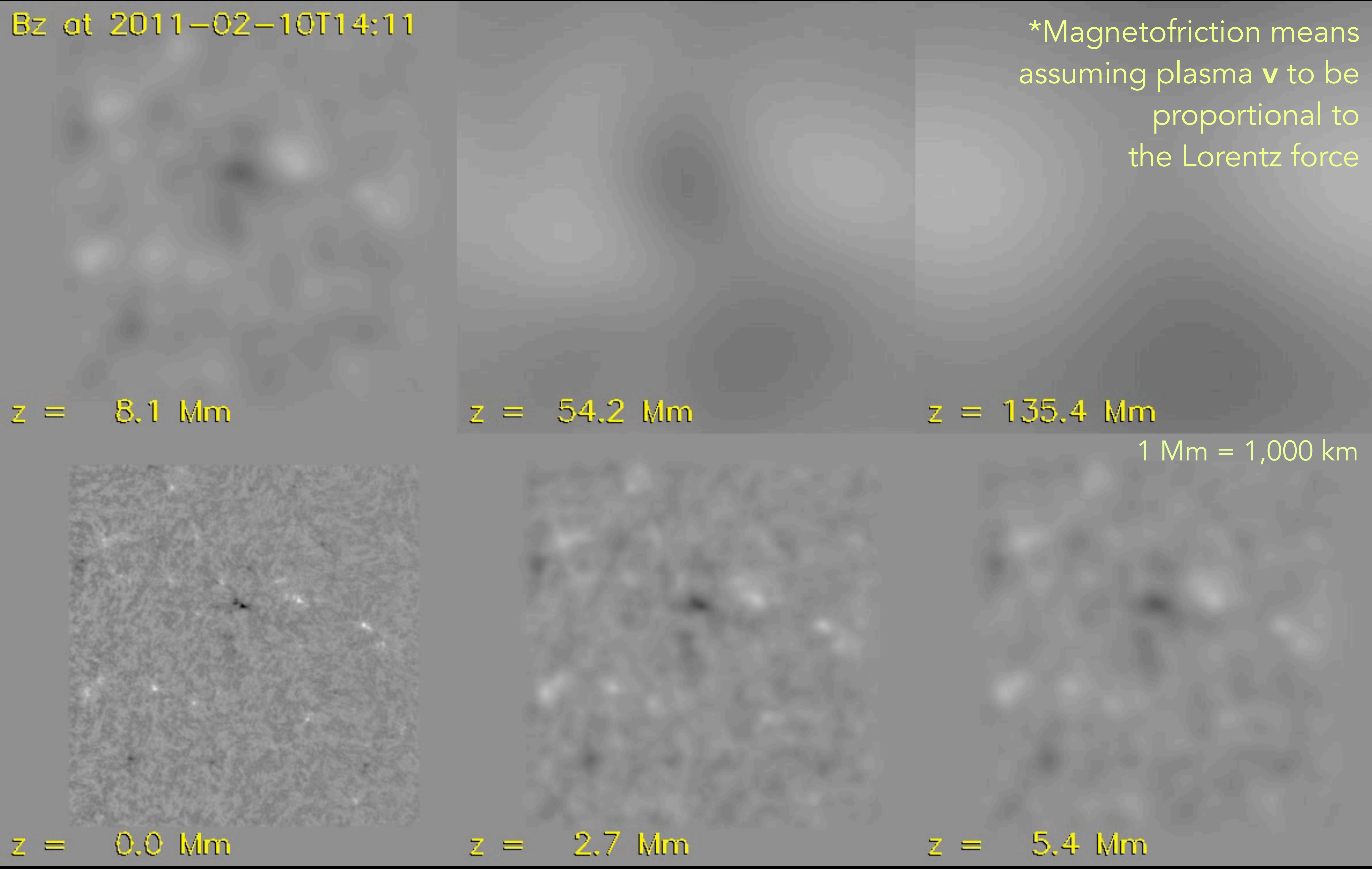

*Magnetofriction means assuming plasma **v** to be proportional to the Lorentz force

1 Mm = 1,000 km

From the CGEM collaboration between UC Berkeley, Stanford and LMSAL (Fisher et al. 2015).

Visualization of field lines based on current density

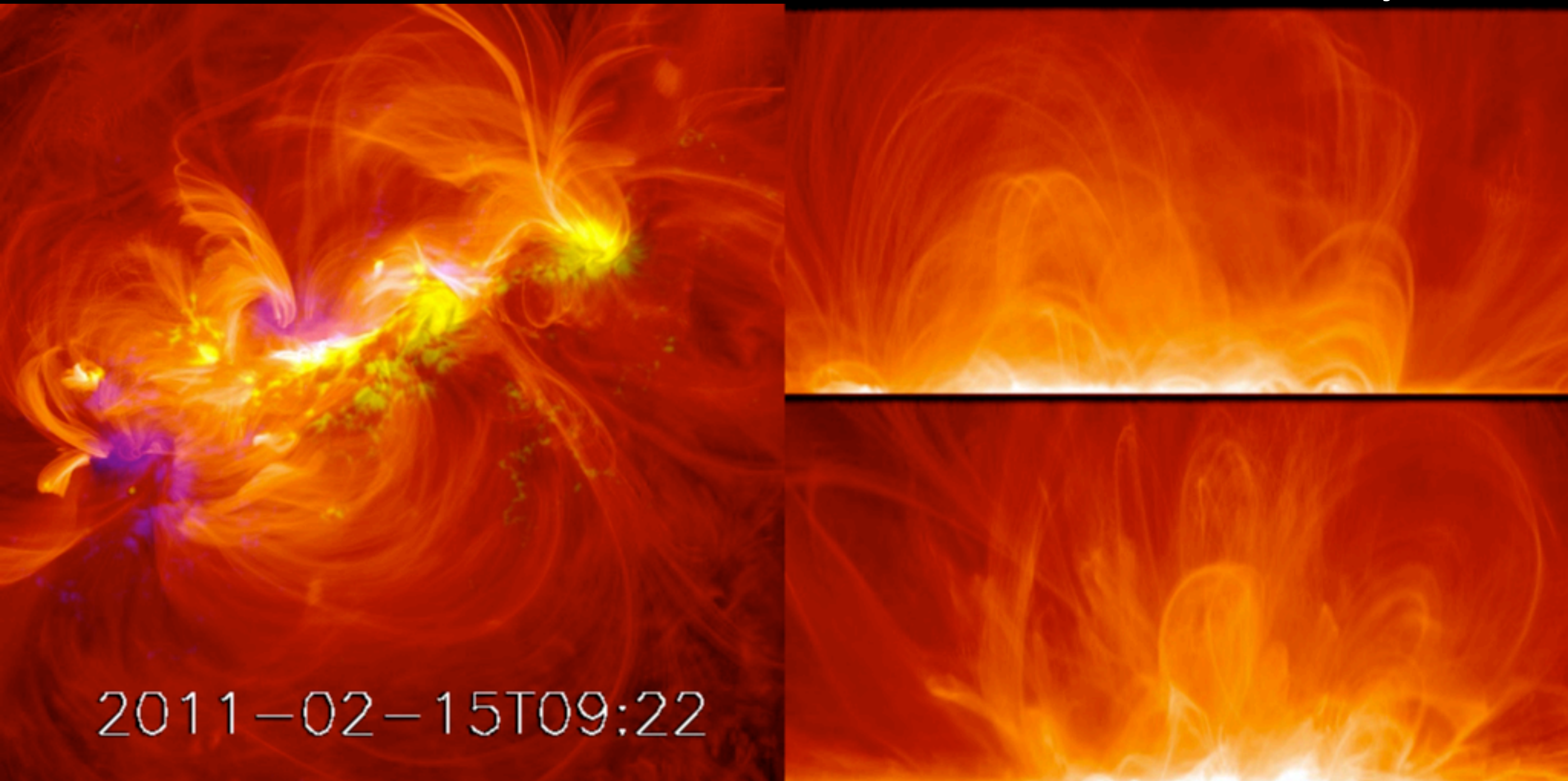

There is no impulsive eruption at the time of the observed X-flare. However, moments before this time, a current-carrying flux rope is observed to form and is eventually ejected, though the rise time is on the order of hours.

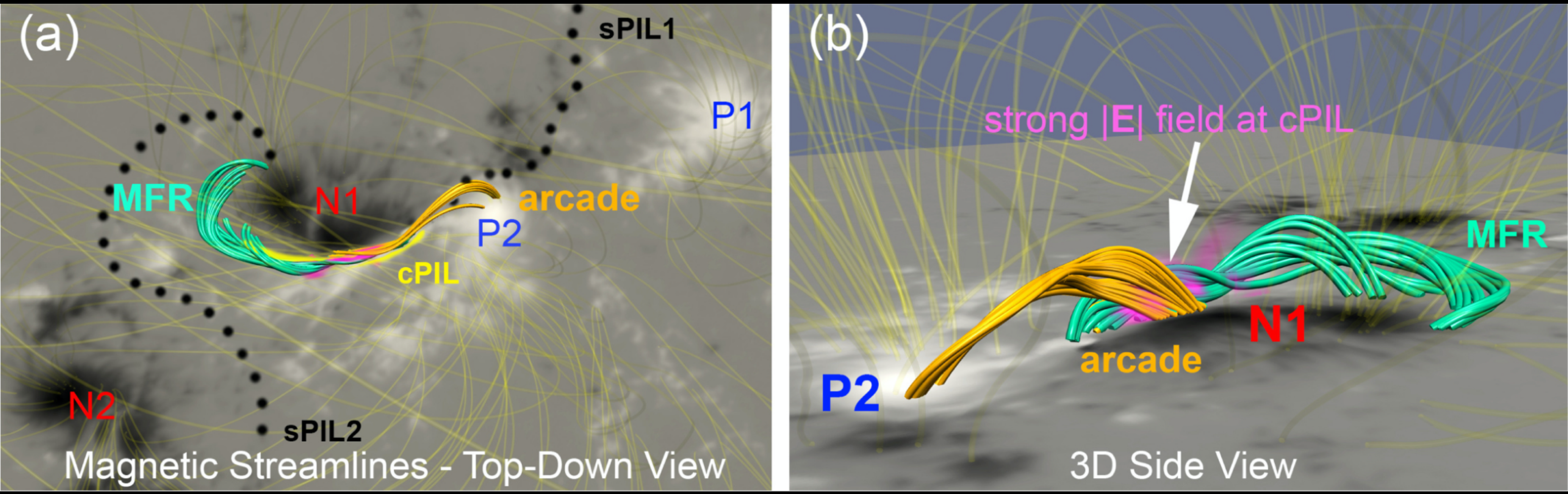

Chintzoglou et al. (2019)

- Collisional polarity inversion line (cPIL) between colliding polarities N1 and P2
- Data-driven MF model shows enhanced E field (proxy of reconnection) above cPIL between arcade field and magnetic flux rope.

Summary and Outlook

- The Sun is a natural laboratory for many astrophysical processes (e.g. heating mechanism of plasmas, acceleration of stellar winds, interpretation of radiative signatures). In particular, a lot of physical information is encoded at EUV wavelengths.
- SDO/AIA has excellent temperature coverage of the corona (quiescent and flaring), and provides critical remote sensing diagnostics to observations by the Daniel K Inouye Solar Telescope (DKIST).
- White light flares not well understood. Usually WL emission is assumed to be black-body radiation @ 10 kK.   What is the WL contribution due to flare loops?
- MHD models of the solar corona increasingly applied to test exoplanet habitability (w.r.t. space weather impacts on life). Are these models valid for other stars?
- Synthetic observables in a data-inspired flare simulation (Cheung, Rempel et al. 2019) qualitatively match observations of flares. For example, non-thermal-like X-ray spectra can result from multithermal distribution of plasma (in our model).
- The SDO dataset is a treasure trove of information for physics-based and for ML models (Bobra & Mason 2018; e-book for ML for Heliophysics; Galvez et al. 2019: A ML Dataset for SDO).